

Very metal-poor galaxies: ionized gas kinematics in nine objects^{*}

A. V. Moiseev,^{1†} S. A. Pustilnik,^{1,4} A. Y. Kniazev^{2,3}

¹ *Special Astrophysical Observatory of RAS, Nizhnij Arkhyz, Karachai-Circassia 369167, Russia*

² *South African Astronomical Observatory, PO Box 9, 7935 Observatory, Cape Town, South Africa*

³ *Southern African Large Telescope Foundation, PO Box 9, 7935 Observatory, Cape Town, South Africa*

⁴ *I. Newton Institute, Chile, SAO branch, Nizhnij Arkhyz, Russia*

Accepted March ?? 2010. Received June NN, 2009

ABSTRACT

The study of ionized gas morphology and kinematics in nine eXtremely Metal-Deficient (XMD) galaxies with the scanning Fabry-Perot interferometer on the SAO 6-m telescope is presented. Some of these very rare objects (with currently known range of O/H of $7.12 < 12 + \log(\text{O}/\text{H}) < 7.65$, or $Z_{\odot}/35 < Z < Z_{\odot}/10$) are believed to be the best proxies of ‘young’ low-mass galaxies in the high-redshift Universe. One of the main goals of this study is to look for possible evidence of star formation (SF) activity induced by external perturbations. Recent results from HI mapping of a small subsample of XMD star-forming galaxies provided confident evidence for the important role of interaction-induced SF. Our observations provide complementary or new information that the great majority of the studied XMD dwarfs have strongly disturbed gas morphology and kinematics or the presence of detached components. We approximate the observed velocity fields by simple models of a rotating tilted thin disc, which allow us the robust detection of non-circular gas motions. These data, in turn, indicate the important role of current/recent interactions and mergers in the observed enhanced star formation. As a by-product of our observations, we obtained data for two LSB dwarf galaxies: Anon J012544+075957 that is a companion of the merger system UGC 993, and SAO 0822+3545 which shows off-centre, asymmetric, low SFR star-forming regions, likely induced by the interaction with the companion XMD dwarf HS 0822+3542.

Key words: galaxies: dwarf – galaxies: interactions – galaxies: kinematics – galaxies: evolution – galaxies: star formation – galaxies: individual: (UGC 772, HS 0122+0743, SBS 0335–052E and W, HS 0822+3542, SDSS J1044+0353, SBS 1116+517, SBS 1159+545, HS 2236+1344, SAO 0822+3545)

1 INTRODUCTION

The group of very rare dwarf galaxies with gas metallicities Z below $Z_{\odot}/10$ (or $12 + \log(\text{O}/\text{H}) < 7.65$, e.g., review by Kunth & Östlin (2000)), are called eXtremely Metal-Deficient, or XMD galaxies. Such objects comprise only about two per cent of known blue compact galaxies (BCGs), low-mass galaxies with active star formation (e.g. Pustilnik et al. 2005a). The latter, in turn, comprise about 6 per cent of the entire local dwarf galaxy population (Lee et al. 2009, and references therein). Thanks

to intensive searches for new XMD galaxies in several recent large surveys, (e.g., Melbourne & Salzer 2002; Ugryumov et al. 2003; Pustilnik et al. 2003c; Kniazev et al. 2003; Pustilnik et al. 2005a; Brown, Kewley & Geller 2008; Papaderos et al. 2008; Guseva et al. 2009, among others, and references therein), the number of currently known such objects in the local Universe is about 100. There is also progress in identification of such objects at large redshifts (Kakazu, Cowie & Hu 2007).

The interest in these *atypical*, local Universe galaxies is caused by the similarity of their properties to low-mass galaxies in the early Universe, when the typical metallicity of galaxies was one-two orders of magnitude smaller than the solar one. Therefore, understanding the specific processes of star formation (SF) and evolution

^{*} Based on observations obtained with the Special Astrophysical Observatory RAS 6-m telescope.

[†] moissav@gmail.com(AVM), sap@sao.ru(SAP), akniazev@sao.ac.za(AYS)

in nearby galaxies with such low metallicity will provide insights into similar processes in young galaxies at high redshifts. To better understand various aspects of XMD galaxies star formation and evolution, we conduct an extensive study of a subsample of XMD galaxies in optical, NIR and radio domains (e.g., Pustilnik et al. 2003a, 2004a; Pustilnik, Kniazev & Pramskij 2004b; Pustilnik, Kniazev, & Pramskij 2005b; Pustilnik & Martin 2007; Ekta, Chengalur & Pustilnik 2008; Pustilnik, Tepliakova & Kniazev 2008; Ekta, Pustilnik & Chengalur 2009).

One of the fundamental questions of SF in low-mass, gas-rich galaxies is the trigger mechanisms of starbursts: whether the intrinsic instabilities in gas discs are capable to produce the observed level of enhanced (bursting) SF (e.g., models by Pelupessy, van der Werf, & Icke (2004) and Di Matteo et al. (2008); observations of Virgo cluster dIrs by Brosch, Almozino, & Heller (2004) and references therein), or external mechanisms (such as tidal disturbances and mergers) are necessary in a significant fraction of observed starbursts.

From the analysis of the density distribution in BCGs in comparison to more typical late-type dwarfs, Salzer & Norton (1999) concluded that the former have a higher gas concentration and, therefore, BCGs represent a special group of galaxies, more susceptible to internal instabilities and related starbursts. But, it is unknown whether this is an inherent property of BCG progenitors, or this higher gas concentration appeared due to a minor merger, or as a result of a recent interaction with a barely detectable companion. If due to mergers or interactions, BCG progenitors could be the quite common late-type dwarfs. To disentangle the possible scenarios one needs a large, representative sample of starbursting galaxies with well studied and understood kinematics of both HI and ionized gas. This is required to determine the prevalence of external or internal disturbances.

First statistical indications for the possible importance of interactions to trigger starbursts in BCG progenitors was presented by Taylor et al. (1995) in their search for HI-rich companions in a small BCG sample. For a larger BCG sample, the conclusion on the high fraction of interaction-induced starbursts was made by Pustilnik et al. (2001a, see also Noeske et al. (2001)), based on the comparison of observed relative distances and ‘threshold tidal distances’, at which a perturber galaxy should induce shocks in the gas disc and produce dissipation of gas angular momentum (as suggested by Icke 1985). While that study was *indicative* of the important role of collisions in *starbursts* of gas-rich low-mass galaxies, more elaborate tests should be used to clear up the real role of external factors in starbursts. In turn, numerous studies of galaxy morphology and kinematics at redshifts of up to ~ 1 (e.g., Puech et al. 2006; Yang et al. 2008) show clear indications on the importance of external mechanisms on the enhanced SF in a significantly larger galaxy fraction than at the current epoch.

In many cases, the traces of interactions can be hidden if only images of stellar components are available. Therefore, gas morphology and kinematics provide a better tracer of interaction-induced starbursts. To this end, HI mapping is a good way for galaxies with sufficiently large HI flux. For less gas-rich and/or more distant galaxies, the study of the

ionized gas kinematics can be a good, complementary technique. Besides, this method provides usually a finer angular resolution and allows comparison of the global gas kinematics derived from HI mapping with the gas motions within the region of higher density, around the sites of SF. These kind of studies, initiated by Östlin et al. (1999, 2001) for a small sample of luminous BCGs, already provide good evidence for merger-induced SF in such objects. Some indications for the same phenomenon have been observed by García-Lorenzo et al. (2008) for a group of five other luminous BCGs and by Pérez-Gallego et al. (2009) for representatives of the similar group of Luminous Compact Blue Galaxies.

The starbursting XMD galaxies are especially interesting in this aspect, since the results may have implications for cosmological young galaxies in the high-redshift Universe. The evidence of significantly disturbed optical morphology and interactions, indicating an unrelaxed state of many XMD galaxies, was already noticed by us (e.g., Pustilnik et al. 2004b, 2005b, 2006) and more recently by Papaderos et al. (2008). How does this relate to the origin of XMD galaxies?

There are several options for evolutionary scenarios of XMD dwarf galaxies, already emphasized in the literature (e.g., Pustilnik et al. 2005b). Two of them relate to gas-rich discs, which are very stable locally, and being isolated, have been evolving very slowly (like LSB galaxies). Some of them might even remain dark objects (e.g., Pustilnik 2008) (and, thus, ‘pristine’ like protogalaxies at epochs of the major galaxy formation). Such galaxies would be very difficult to discover/recognise before they (by chance) have experienced a strong external perturbation due to an interaction with a galaxy-sized mass. When this happens, such galaxies can lose their global stability and experience a substantial SF burst. Due to their slow evolution, during the starburst they would appear as gas-rich and very metal-poor (XMD) objects. Therefore, the study of gas kinematics for the sample of XMD galaxies can shed light on their origin as a group, or can give clues to the diversity of their properties and their finer classification.

In this paper we present the results of an $H\alpha$ study of the ionized gas kinematics in nine XMD starbursting galaxies (BCGs) conducted with the SAO 6-m telescope’s scanning Fabry-Perot Interferometer (FPI). These galaxies constitute a part of a larger XMD galaxy sample, for which we conduct a multiwavelength study of their properties. Most were selected for this FPI $H\alpha$ study due to their unusual or disturbed optical morphology. For a fraction of them, the HI mapping data are available, which provide an opportunity of the combined view on the gas kinematics. We plan to continue this project for a larger sample of XMD starbursting galaxies in order to improve statistics and to search for possible differences in the properties of the ionized gas kinematics.

Due to volume limitations, the scope of this paper is kept mainly to observational results for the studied XMD galaxy subsample and their preliminary analysis. The more advanced analysis, involving multiwavelength data and new methods of modelling (like suggested by Barnes & Hibbard 2009), will be presented for individual galaxies in forthcoming papers. This paper is organised as follows: in Sect. 2 we describe observations and their reduction. Sect. 3 presents

Table 1. Log of the 6-m telescope FPI observations

Object	Date	Exposure time (s)	ang. resol. (arcsec)
(1)	(2)	(3)	(4)
SDSS J0113+0052	11.01.07	36x200	4.0
HS 0122+0743	10.01.07	2x36x90	2.3
SBS 0335-052W	14.01.08	2x36x150	1.4
SBS 0335-052E	14.01.08	2x36x150	1.4
HS 0822+3542	10.01.07	36x250	1.4
SDSS J1044+0353	14.01.08	36x150	1.4
SBS 1116+517	10.01.07	36x250	1.5
SBS 1159+545	14.01.08	36x170	1.8
HS 2236+1344	08.09.05	36x250	1.0

the description of data analysis and the summary of results. In Sect. 4 the kinematic properties are discussed in more detail and are compared with other data on these BCGs, and their likely interpretation is suggested. Sect. 5 summarises conclusions of this study.

2 OBSERVATIONS AND DATA REDUCTION

The observations of XMD galaxies were conducted with the multimode instrument SCORPIO (Afanasiev & Moiseev 2005) installed in the prime focus of the SAO 6-m telescope (BTA) during 3 runs (see Table 1 for details and Table 2 for galaxy main parameters). The desired spectral interval in the neighbourhood of the redshifted H α line was cut using a set of narrow-band filters ($FWHM = 15 - 20\text{\AA}$). The width of the free spectral interval between the neighbouring orders of interference was equal to 13\AA (about 600 km s^{-1}). The resolution of the interferometer ($FWHM$ of the instrumental profile) was 0.8\AA (35 km s^{-1}) for a $0.36\text{\AA}/\text{channel}$ sampling. The detector was a 2048×2048 EEV 42-40 CCD operating in the 2×2 and 4×4 (for SDSS J0113+0052=UGC 772 and HS 0122+0743) pixel instrumental averaging mode in order to reduce the readout time. The corresponding image sampling was $0''.36$ and $0''.72\text{ pixel}^{-1}$ respectively. The resulting field of view has a size of $6'.1$. In column 4 we also present the final angular resolution of our data which is a combination of the real seeing and the data reduction smoothing.

We took a total of 36 successive interferograms per object with different gaps between the plates of the FPI. The observational data were reduced using an IDL-based software package (Moiseev 2002; Moiseev & Egorov 2008). After primary reduction, night-sky line subtraction, and the wavelength calibration, the observations were reduced to the form of a data cube, where each pixel in the field of view contains a 36-channel spectrum. We removed the ghost images that appear in the plates of the interferometer using the algorithms described by Moiseev & Egorov (2008). To check the quality of ghosts removal on the data of extended objects, we observed HS 0122+0743 and SBS 0335-052E,W successively in two fields turned in the position angle.

We fitted the H α emission profiles to the Voigt function, which in most cases describes the observed contour fairly

well (see discussion in Moiseev & Egorov 2008). The profile fitting results were used to construct the two-dimensional field of line-of-sight velocities of ionized gas, the map of velocities dispersion, and images of the galaxy in the H α line and in the neighbouring continuum. We estimate the accuracy of line-of-sight velocity measurements through the measured S/N ratios, using the relations given in Fig. 5 of Moiseev & Egorov (2008). The accuracy was found to be $1-5\text{ km s}^{-1}$ in the bright HII regions and amounts to $10-15\text{ km s}^{-1}$ in the regions with the minimal surface brightness, where the emission line shows up at the S/N ratio level of $S/N \approx 5$. In Fig. 1 we show the examples of representative H α -line profiles for three program galaxies SBS 0335-052W and E and SBS 1116+517.

3 RESULTS AND ANALYSIS

In Table 2 we present the summary of the main observational parameters of the studied XMD galaxies. Since the accuracy of our total H α flux estimates (10-30 per cent) is in general worse than that for dedicated H α photometry, we give our values only for unknown H α fluxes. For the remaining objects, we cite data from the literature. Absolute magnitudes, M_B , are calculated for distances taken from NED¹, except for HS 0822+3542 and its companion LSB dwarf. As discussed in Pustilnik et al. (2010), they are situated in the region with large peculiar negative radial velocities ($\sim 300\text{ km s}^{-1}$) due to the effect of the huge Local Void (Tully et al. 2008). So to derive their distances, this peculiar velocity was accounted for.

The dominant or important mode of gas motions in late-type, low-mass isolated galaxies (even for objects with luminosities corresponding to M_V fainter than -14.0) is rotation in a gravitational field of a Dark Matter (DM) halo and baryonic disc (e.g., Begum et al. 2006, 2008, and references therein). Two types of processes can significantly affect the regular velocity field attributed to rotation: the star formation activity and tidal interactions.

3.1 Kinematics of SF induced shells

The strong SF activity releases a significant amount of kinetic and thermal energy in short periods, and it results in the formation of hot bubbles and shells with typical sizes of a hundred pc to about one kpc. Such shells, with maximal observed line-of-sight velocities in the range of ten to a hundred km s^{-1} are recognised in both long-slit spectra and 2D H α velocity fields of star-forming galaxies (e.g., Martin 1996, 1998; Zasov et al. 2000; Pustilnik et al. 2003b; Lozinskaya et al. 2006; Martinez-Delgado et al. 2007; Bordalo et al. 2009, among others). In principle, the large-scale velocity fields in such expanding ionized shells are sufficiently simple. However, in case of dwarf galaxies, which have relatively small rotation velocities, shells can significantly perturb the disc velocity field. In Appendix A we present the simulated velocity field of dwarf galaxies with

¹ <http://nedwww.ipac.caltech.edu/>

shells for several simple cases. Using the characteristic parameters typical of our sample (disc size, inclination, rotation curve, etc.), we describe the technique for such shells recognition and masking in the observed velocity fields. Fortunately, in many simple theoretical scenarios it is possible to extract the real parameters of global rotation, even when the shell expansion velocity is larger than the line-of-sight projection of global rotation on given radii.

3.2 External perturbations of velocity fields

It is not yet well understood how the strength of starbursts and that of related expanding bubbles are connected with internal or external triggers. But, since the external perturbations (e.g., due to galaxy collisions or extragalactic cloud infall) provide disturbances which are additional to internal ones, they are naturally expected to trigger the stronger disturbances in galactic gas and to result in more intense star formation. Besides, in general, the characteristic timescales of singular star-forming events in isolated low-mass galaxies (of ten to several tens Myr) are shorter than those for the events induced by external interactions. The latter are comparable to rotation periods, and usually are of the order of a hundred Myr and more, the typical timescale for galaxy response to a collision-induced perturbation (e.g., Di Matteo et al. 2008, and references therein).

This is due to different spatial scales involved in such SF episodes. For internal perturbations we usually have some local enhancement, while for external ones the gas flows on scales of the whole galactic disc are involved. Therefore, one can expect rather different effects in isolated and interacting starbursting galaxies. In the former, the gas velocity field should display the characteristic rotation pattern with rather localised disturbances due to the starburst-related shells. More or less typical dIrr galaxies can serve as templates for such kinematics. In the interaction-induced starbursts one can observe, besides the overall rotation and the appearance of shell kinematics, the effects of tidally disturbed velocity fields to various degrees. In extreme cases of a major merger, the strong disturbance of the initial equilibrium rotation field can almost wash out the regular component.

Apart from non-destructing (fly-by) collisions, various types of mergers (major, intermediate mass-ratio, and minor [$M_1:M_2 > 5$]) can trigger late-type galaxy starbursts. Depending on the stage and mass proportion, the velocity fields can show various patterns – from very disturbed with no traces of regular rotation to more or less regular rotation with residual motions (e.g. counter-rotation in the central region, where a smaller component has sunk as the result of minor merger). As recent simulations demonstrate (e.g., Kronberger et al. 2006; Pedrosa et al. 2008), the bifurcations in velocity curves should appear (that is prominent asymmetries in receding and approaching branches of rotation curves) as a result of close recent encounters. Various appearances of complex velocity fields resulting from major mergers of disc galaxies were demonstrated by Jesseit et al. (2007).

3.3 Fitting results

From the above discourse it is clear that it is quite natural to analyse H α velocity fields in the studied XMD dwarf galaxies by trying to fit them with a model of a flat rotating disc and to compare the residual velocity field against various patterns characteristic of shells, warps, central counter-rotation, discontinuities, etc. Of course, the morphology of both stellar continuum and H α emission should be taken into account in the course of the results' interpretation.

We analysed the velocity fields using the well-known approximation of a thin rotating disc ('tilted-rings' method), which is generally accepted in analysis of gas kinematics. For the method description and references to the original works, see Moiseev et al. (2004). This method calculates the disc orientation parameters (major axis position angle PA , inclination i , systemic velocity V_{sys}) together with radial variations of the rotation velocity V_{rot} . In special cases of non-circular motions, we can also estimate radial dependencies of PA and V_{sys} .

In Table 3 the 'best-fitting' model parameters are summarised: systemic velocity V_{sys} , position angle PA and inclination angle i , along with relevant brief comments. Unfortunately, from the kinematic model we could only derive i for three galaxies, whose inclinations are indicated with errors in the Table 3. For J0113+0052 and SAO 0822+3545, we adopted the inclinations from published HI maps. In the remaining cases, to estimate the inclination angle we adopted the approach based on the morphology of the overall H α emission and the observed ratio of minor to major axis of H α 'ellipsoid' $p=a/b$. Assuming that this reflects the real gas distribution for an inclined 'thick' (typical of dwarf galaxies) disc with the intrinsic axial ratio q , we estimated the inclination i with well-known formula $[\cos(i)]^2 = (p^2 - q^2)/(1 - q^2)$. The estimate of parameter q was adopted according to formula A6 from Staveley-Smith, Davies & Kinman (1992). We understand that in many cases, where we infer strong disturbances in morphology and velocity field, the above assumption can be hardly justified, and hence the adopted inclination angle and the related amplitude of rotation velocity can be rather uncertain. But the concrete choice of i does not affect the overall radial dependence of the model rotation velocity. A more detailed description of the data and their model fits, along with discussion of relevant kinematics and morphology in HI-line and other points are presented for each individual galaxy in Section 4.

For each of the nine program XMD galaxies and for two 'by-product' LSB dwarf galaxies, we show the related graphic materials in Figures 2-4. The colour images of velocity field data are available in electronic version of the journal. They are arranged in columns of 6 images in the following order. The first (top) panel displays continuum image in g -filter from the SDSS or in the blue band from the digitised Palomar Observatory Sky Survey (POSS). For SBS 0335-052E,W, the BTA B -band images are used from Pustilnik et al. (2004b). The brightness distribution is shown in logarithmic scale. The second panel shows the image of integrated emission in the H α line in logarithmic scale. The third panel shows the velocity field, both in colour and by isovelocity lines. In the forth panel, we show the 'best-fitting' model of thin tilted rotating disc. The fifth panel presents, in colour, the residual velocity field (observed mi-

Table 2. Parameters of nine XMD and two by-product (below the line) galaxies

IAU name	Coord. (2000.0)		$V_{\text{hel}}^{\clubsuit}$ km s ⁻¹	$B_{\text{tot}}^{\ddagger}$ mag	M_B^{0*} mag	O/H [†]	F(H α) [§]	$D^{\S\S}$ Mpc	Scale pc arcsec ⁻¹	Alternative name
	R.A. h m s	Dec. ° ′ ″								
(1)	(2)	(3)	(4)	(5)	(6)	(7)	(8)	(9)	(10)	(11)
SDSS J0113+0052	01 13 39.40	+00 52 27.9	1176± 1	16.28 ¹	-14.70	7.24	6.8	16.3	79	UGC 772
HS 0122+0743	01 25 34.18	+07 59 22.2	2940± 2	15.48 ²	-17.76	7.63	20.0 ²	40.3	195	UGC 993
SBS 0335-052W	03 37 38.46	-05 02 36.3	4038± 2	19.14 ⁴	-14.73	7.12	1.4 ⁴	53.8	261	
SBS 0335-052E	03 37 44.04	-05 02 37.6	4053± 2	16.95 ⁴	-16.92	7.29	32.0 ⁴	53.8	261	
HS 0822+3542	08 25 55.43	+35 32 31.9	727± 2	17.92 ³	-12.49	7.45	7.6 ⁶	13.5	65	
SDSS J1044+0353	10 44 57.84	+03 53 13.2	3865± 1	17.62 ⁵	-16.20	7.44	14.5	53.8	261	
SBS 1116+517	11 19 34.29	+51 30 10.7	1342± 2	17.14 ⁵	-14.70	7.51	15.2	23.1	112	Arp's
SBS 1159+545	12 02 02.36	+54 15 50.1	3592± 1	19.00 ⁵	-14.60	7.49	5.5	52.2	255	
HS 2236+1344	22 38 31.15	+14 00 28.6	6162± 2	17.88 ²	-16.90	7.50	12.0 ²	86.4	419	
Anon J012544+075957	01 25 44.18	+07 59 57.0	3012± 3	17.0 ²	-16.30		1.5	40.3	195	
SAO 0822+3545	08 26 05.59	+35 35 25.7	742± 2	17.56 ³	-12.85		0.4	13.5	65	

(\clubsuit) - systemic velocity on our H α data. For UGC 993 this is a mean of V_{sys} for E and W components; for SAO 0822+3545 - this is HI velocity from Chengalur et al. (2006)

(\ddagger) - Photometry data are from: ¹ Smoker, Davies & Axon (1996); ² Pustilnik et al. in prep.; ³ Pustilnik et al. (2003a);

⁴ Pustilnik et al. (2004b); ⁵ NED/SDSS transformed from g, r to B , ⁶ Moustakas & Kennicutt (2006) for H α flux.

(\dagger) - in units 12+log(O/H). Data are from Ugryumov et al. (2003), Kniazev et al. (2003), Izotov & Thuan (2007), Izotov, Thuan & Guseva (2005).

(*) - corrected for A_B (according to Schlegel, Finkbeiner & Douglas (1998)), with distances from Col. 9

(\S) - in units of 10⁻¹⁴ erg cm⁻² s⁻¹; H α fluxes adopted from literature are coded as photometry data.

($\S\S$) - from NED [Virgo-infall; H₀=73], except HS 0822+3542/SAO 0822+3545, for which additional correction is adopted (see text).

Table 3. Parameters of model rotating discs for observed galaxies

IAU name	V_{sys}	$PA(^{\circ})$	$i(^{\circ})$	Brief comments
(1)	(2)	(3)	(4)	(5)
J0113+0052	1173± 1	199±5	40*	UGC 772. S component is detached. Probable minor merger
0122+0743W	2953± 2	295±5	37±4	UGC 993W, component of major merger in contact
0122+0743E	2927± 2	285±5	69	UGC 993E, component of major merger in contact
0335-052W	4038± 2	64±8	37±9	centre between two knots, W comp. of major merger on HI data
0335-052E	4053± 2	53*	37	counter-rotation core, expanding shell, E comp. of major merger on HI data
0822+3542	727± 2	51±7	31±15	HI and H α motions are decoupled
J1044+0353	3865± 1	273±6	51	distorted kinematics of E-half of the disc
1116+517	1342± 2	-22±7	50	lack of regular rotation, probable major merging remnant
1159+545	3592± 1	-13±5	38	probable merger
2236+1344N	6176± 2	165±30	31	component of major merger in contact
2236+1344S	6164± 1	150±10	35	component of major merger in contact
J012544+075957	3012± 3	324± 7	64	probable companion of UGC 993
0822+3545	742± 4	105*	63*	companion of HS 0822+3542.

(*) - values taken from published HI maps.

nus model) and in the sixth panel the velocity dispersion is shown in colour. For both panels the intensity of H α -line is superimposed by contours. The radial dependence of V_{rot} for the ‘best-fitting’ models of the program galaxies is presented in Fig. 5.

4 DISCUSSION

The issue of strong interactions of star-forming galaxies in the aspect of their evolution is actively studied in recent times (e.g., Puech et al. 2006; Yang et al. 2008; Di Matteo et al. 2008, and references therein). Also, many

N-body simulations are performed to allow both qualitative and quantitative (with more detailed data) classification of observed velocity fields to originate due to strong interactions or mergers (e.g., Kronberger et al. 2006; Jesseit et al. 2007). There is also substantial progress in morphology analysis to assign galaxies to merger products (Conselice 2003; Lotz et al. 2008, and references therein).

The main goal of these FPI H α study was to search for the possible appearances of unusual, highly disturbed, asymmetric velocity fields in the ionized gas kinematics. The latter might indicate sufficiently strong interactions or various stages of minor or major mergers. This would allow us to make the first step to quantify the role of interactions in

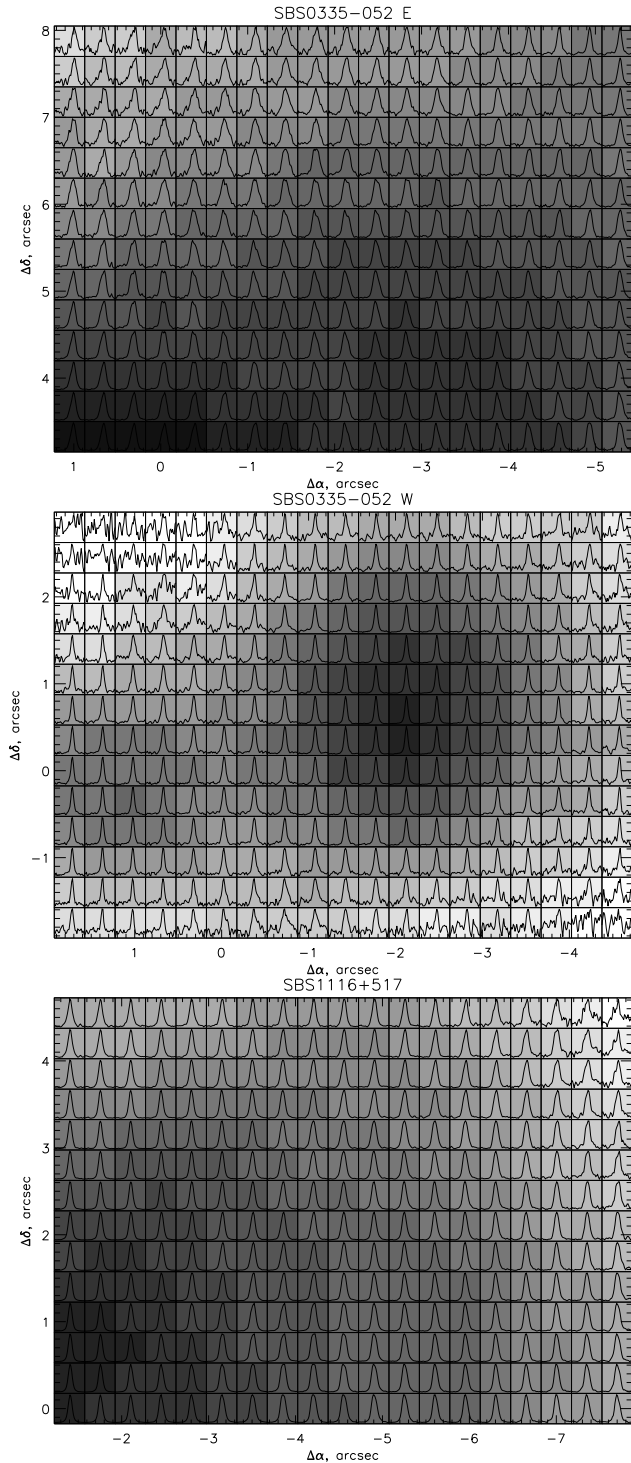


Figure 1. Typical individual H α -line profiles for each spatial resolution element, superimposed on the grey-scale brightness distribution in H α -line. The figure demonstrates the range of S/N ratios and of the line widths. **Top panel:** the region NW of the brightest region in galaxy SBS 0335–052E. Broadened and double-component structures of H α -line profiles are apparent in the regions where Izotov et al. (2006) found the evidence for outflows from the similar line structures. However, our velocity resolution is somewhat insufficient to derive the reliable parameters of the second component. **Middle panel:** almost the full region of galaxy SBS 0335–052W. The hints of the line broadening are seen in the outer LSB regions. **Bottom panel:** the NW part of galaxy SBS 1116+517. There are also indications on the line broadening at the outermost parts of the nebulosity.

active SF of XMD galaxies. Of course, in some cases, the use of only H α kinematics data can be insufficient to distinguish recent interactions from other types of kinematic disturbance. However, the combination of ionized gas kinematics with various morphology indicators, and the use of HI maps (when they are available), or even of integrated HI profiles (Conselice 2006), can lead to the correct classification.

A complementary study of a subsample of XMD galaxies with similar goals was conducted based on GMRT HI mapping, and the first results are presented in Ekta et al. (2006, 2008), Chengalur et al. (2006), Ekta et al. (2009). Some earlier results of HI mapping of XMD starbursting galaxies with VLA were presented by van Zee et al. (1998) for I Zw 18 and Pustilnik et al. (2001b) for SBS 0335–052E,W. The H α kinematics of ionized gas in the prototype XMD galaxy I Zw 18 was analysed by Petrosian et al. (1995). All these data evidence for importance of interactions in the current starbursts of studied XMD galaxies.

If we consider the star-forming or blue compact galaxies (BCGs) in general, there are very few 2D studies of H α kinematics. However, for the majority of them, the morphology data indicate strong disturbances in the outer parts. For some of them, such as II Zw 40, there is clear evidence of a recent merger. Several *luminous* BCGs were studied by Östlin et al. (1999) via imaging in several bands and through H α kinematics with FPI. These authors concluded that all of their galaxies are best treated as being in the stage of merging.

It is worth noting, that in such type of studies, the knowledge of the gas kinematics in the outer parts of a disc can be crucial. In particular, a good illustration is the luminous BCG Arp 212 (III Zw 102). For this galaxy, García-Lorenzo et al. (2008) obtained the ionized gas velocity field for the circumnuclear region from integral-field spectroscopy with *INTEGRAL* fiber-based system. From these spatial limited data, they suggested that the galaxy “shows a velocity field resembling a rotational system”. However, the large-scale H α velocity field taken with FPI, revealed a more complex picture where the outer HII regions belong to a warped polar ring, formed via the external gas accretion (Moiseev 2008). We emphasize that the spatial coverage in our study for all program galaxies, due to the large SCORPIO field-of-view, was sufficient to include their distant periphery. Thus we do not miss any substantial gas velocity field deviations, as long as they have H α emission above the detection threshold.

First, we discuss the analysis and model fitting of H α for each XMD galaxy individually (along with available HI maps for some of them), and then, we summarise our conclusions for the subsample as a whole.

4.1 UGC 772 = SDSS J0113+0052

This galaxy has quite a large extent (~ 1 arcmin) and very complex morphology and kinematics. Observations were obtained at rather poor seeing of ~ 4 arcsec, but this was sufficient for general characterisation and modelling of its velocity field. The seeing probably has somewhat affected the picture for the ‘S knot’, which has a total extent of $\sim 20 \times 10$ arcsec. The optical light, both in broad-band continuum and in H α , shows clearly two distinct components.

The larger one (or the main body) with the overall extent of $\sim 50 \times 20$ arcsec is elongated at $PA \sim 60^\circ$ and contains three HII regions, each having some elongation and/or sub-structure. Izotov & Thuan (2007) obtained spectra for 3 HII regions in the main body on one slit. Their values of O/H in all three regions are consistent to each other within the cited errors and can be treated as O/H for the whole main body. We estimated that the weighted mean for those three O/H values corresponds to $12 + \log(O/H) = 7.29 \pm 0.05$. The general velocity gradient in the main body is along the NS direction, that is almost perpendicular to the major axis of symmetry.

The centre of the second distinct component (hereafter, UGC 772 S) is situated ~ 35 arcsec (or ~ 2.8 kpc at the adopted distance of 16.3 Mpc) south of the geometrical centre of the main body. This is also elongated in both continuum and $H\alpha$, roughly in the NS direction and has a clear structure. There are no published measurements of O/H for this region. Our recent spectrum of this region at the SAO 6-m telescope (Pustilnik et al., in preparation) results in $12 + \log(O/H) = 7.38 \pm 0.07$. Despite this O/H being somewhat larger than that in the main body, the errors of both values are too large to claim a real difference. The general velocity gradient along the EW direction (about minor axis) is clearly seen in this component.

The velocity dispersion is rather low ($10\text{--}20 \text{ km s}^{-1}$) in all HII-regions around current SF sites, where the intensity of $H\alpha$ show local peaks. The latter is common for the majority of other studied SF galaxies. It reaches values of $40\text{--}50 \text{ km s}^{-1}$ in several low-brightness small periphery knots, where this enhancement is probably related to shocks in expanding shells.

To zeroth order, the tilted-ring model is a reasonable approximation for the global motions in this object over the full range of the observed velocities. However, since the distribution of $H\alpha$ emission has a huge gap between the main body and the S component, it is difficult to find a good fit based only on our FPI data. The GMRT HI velocity field for this object from Ekta et al. (2008), which shows consistent features with our $H\alpha$ velocity field in the overlapping regions, is helpful for the choice of the best-fitting model. Therefore we accepted the value of disc inclination from those HI maps. The next parameters – the systemic velocity of kinematic centre, and the PA of major kinematic axis were derived from our $H\alpha$ data. There is no well defined photometric centre. Therefore, the rotation centre was determined only from the symmetry of the velocity field. Its position also agrees (within a few arcsec) with the centre of HI distribution and rotation as it follows from the GMRT data. A model was constructed only for $r > 12$ arcsec; since in the inner region the number of points with the measured velocities is small and we fail to construct the stable model. In the outer regions the circular rotation model fits well the observed velocity field. The values of residual velocities in general do not exceed $5\text{--}10 \text{ km s}^{-1}$, reaching $\pm 15 \text{ km s}^{-1}$ in several regions. The latter are still smaller than the observed amplitude of the rotation curve (18 km s^{-1}). The largest non-random residual velocities (both negative and positive) are seen in the region of UGC 772 S. This looks like a more or less systematic gradient with the full range of $\sim 30 \text{ km s}^{-1}$.

Due to the patchy structure of ionized gas and the ev-

ident problems with a simple modelization of its global velocity field, it is important to compare the $H\alpha$ velocity field with a lower resolution, but much better sampled motions of HI as seen, e.g., in HI maps obtained with GMRT in Ekta et al. (2008). In particular, as well seen in their Fig. 9 (right) for the FWHM beam of 15×10 arcsec, the gas velocities observed in HI, in both the main body and UGC 772 S, correspond well to those measured in $H\alpha$. The general direction of the HI velocity gradient is close to NS within the main optical body in accord with the ionized gas motions. However, one can see strong deviations of HI velocities near UGC 772 S (and the related HI-density peak), and in the southern part of the HI ‘disc’. They look like an additional, smaller velocity component with the gradient being roughly along the EW direction. The other indications on the strong tidal HI protrusions are seen in their map in Fig. 9 (left). The $H\alpha$ velocity field in UGC 772 S also shows a gradient close to the EW direction, and thus, ionized gas motions are coherent with those of HI. These kinematically and spatially decoupled components of UGC 772 suggest that we are witnessing a dwarf galaxy merger stage (the main body of UGC 772 and UGC 772 S), probably close to coalescence. An alternative interpretation of the region UGC 772 S as a supergiant HII region on the edge of a dwarf galaxy looks quite improbable due to three facts: (i) the strong disturbance of the overall HI morphology, (ii) the occurrence of the galaxy’s highest HI density peak in the edge region is very unusual for an isolated galaxy, and (iii) the velocity field in this region is clearly detached from the main galaxy motions.

UGC 772 is situated in a small group of gas-rich galaxies (e.g., Ekta et al. 2008). Therefore, such galaxy collision looks quite probable. The current starburst in UGC 772 and in this smaller southern ‘companion’ galaxy is then most probably triggered by their collision.

4.2 UGC 993 = HS 0122+0743

This is one more rather extended object with very complex morphology and kinematics. The body, in both continuum and $H\alpha$, represents a group of seven bright knots (SF regions) superimposed on a LSB component. They are visually joined into two aggregates of similar size. The velocity field looks rather regular with two regions of clear gradient with the same direction and sign and the velocity ranges of ~ 100 and $\sim 60 \text{ km s}^{-1}$. The regions roughly correspond to the W and E parts of the body. The velocity dispersion in most of the galaxy body, and in particular, around the SF knots, is quite low: $\sim 10\text{--}30 \text{ km s}^{-1}$. As in the previous galaxy, it is enhanced up to $50\text{--}60 \text{ km s}^{-1}$ in several areas between HII regions.

Guided by its morphology and the appearance of its velocity field, we model this object with two rotating discs in contact (see Figure 2). The first component, on the western edge, is fitted with $V_{\text{sys}} = 2953 \pm 2 \text{ km s}^{-1}$, $PA = 295^\circ \pm 5^\circ$, and with model-derived $i = 37^\circ \pm 4^\circ$. Maximal rotation velocities (after inclination correction) reach $\sim 30 \text{ km s}^{-1}$. The second component, at the eastern edge, is best modelled with $V_{\text{sys}} = 2927 \pm 2 \text{ km s}^{-1}$, $PA = 285^\circ \pm 3^\circ$, and $i = 69^\circ$ (estimated from its axial ratio). For this component, the inclination corrected, maximal rotation velocity reaches $\sim 50 \text{ km s}^{-1}$. Resulting residual velocities appear rather small ($\lesssim 8 \text{ km s}^{-1}$)

in most of the mapped area. The largest positive values of residuals are seen south of the bright HII region of the western component and on the NW of the eastern component. They may be the tracers of current interaction or outflows. The two prominent, but relatively compact regions of negative residuals (near the kinematic centre and near the SE edge) in the eastern component can be related to shells around recent starbursts. Or alternatively, the latter can be the tidally disturbed gas with counter-motion relative to that at the NW edge. For the case of modelling UGC 993 by a single rotating disc (as the first guess), the overall residual velocities were by a factor of two and more larger.

The recent HI maps obtained at GMRT (Ekta et al. 2009, in preparation) show clear evidence of disturbed structure, with the large low-density HI plume stretching to the angular distance of ~ 1 arcmin to the south of a denser HI envelope that covers the optical body of the galaxy. The whole HI gas shows very complex kinematics. In the regions, where the H α emission is well traced, HI displays the velocity pattern similar to that presented here in H α .

All available morphology and kinematics data suggest that in UGC 993, we are witnessing a rather rare case of dwarf galaxy encounter in contact, when they have well traced regular velocity fields of both components. The kinematic data suggests that the real distance between the colliding galaxies is significantly larger, and their visible contact is due to projection effects. The strong SF activity in many HII regions, presumably triggered by the recent strong interaction, is spread over the components' bodies.

From the model fit of the observed velocity field, the deprojected rotation velocity in the E component is a factor of ~ 1.6 larger, and hence, its estimated total mass should be also significantly larger. If the Tully-Fisher scaling is valid for the two discs in collision ($M \propto V^{3.5}$), the E component can be ~ 5 times more massive. This would imply a case of minor merger. However, rather similar sizes of the two galaxies in question (as best followed namely through H α velocity field) and a strong HI tidal plum mentioned above, are strong evidence for a major merger. The above large difference in rotation velocities can be due to two factors: (i) not properly correcting for inclination angle in the W component, (ii) the velocity fields themselves are affected by strong interactions, so the Tully-Fisher relation may be not applicable. To construct a more self-consistent model, one needs to combine both H α and HI velocity fields, as well as some additional photometry including near-IR data. This will be attempted in a forthcoming analysis.

4.3 The system SBS 0335–052E,W

The SF galaxy SBS 0335–052W is the most metal-poor gas-rich object with an O/H range in different knots between $6.9 < 12 + \log(\text{O}/\text{H}) < 7.22$ (Izotov et al. 2009). With SBS 0335–052E (at 22 kpc in projection, Pustilnik et al. 2001b) it comprises a unique pair of interacting/merging gas-rich dwarfs with the lowest metallicities. Both galaxies show unusually blue stellar population in the outer parts of their optical images (Pustilnik et al. 2004b). The ratio $M(\text{HI})/L_B \sim 5$ for SBS 0335–052W is one of the greatest known. The recent detailed study of its disturbed HI kinematics and morphology with GMRT is presented by Ekta et al. (2009). It suggests a merger of extended gas bodies soon after the first en-

counter. However, the denser central regions of both galaxies, with regions of current SF and surrounding ionized gas, are separated at a significant distance, and can be thus less susceptible to an external disturbance. Therefore, one can hope that kinematics of their innermost ionized gas can keep information on galaxy original rotation. Due to the recent close encounter between E and W galaxies, the gas motions are significantly affected by the tidal torques, especially in the outer parts of colliding galaxies. On the other hand, the gas kinematics in the innermost parts can be affected by current/recent SF episodes.

One of the important issues in understanding this unusual interacting pair is the following: why do the optical luminosities and SFRs of E and W galaxies differ by an order of magnitude, while their global HI properties are pretty similar? In principle, the substantial part of the answer can be related to differences in the geometry of collision for two components and the related strength of tidal action. Indeed, the high resolution GMRT maps of the innermost HI gas give evidence for a significant difference in the main velocity gradients in E and W galaxies. For the orbital plane sky projection close to the EW direction, the collision of the E galaxy is closer to a retrograde one. Meanwhile, the innermost velocity field of the W galaxy, having its main gradient in the N-S direction, corresponds to an almost polar collision. This would imply a less effective tidal perturbation. Our FPI H α velocity field allows a consistent check of the HI data.

4.3.1 SBS 0335–052W

The observed ionized gas velocity field of the W galaxy looks like a combination of two components. One, centred at the bright HII region, shows a very small gradient, with an amplitude of less than $\sim 10 \text{ km s}^{-1}$ and the direction close to N–S. The other reflects the gas motion between two peaks of H α emission (mainly in E–W direction) and has the amplitude of $\sim 20\text{--}25 \text{ km s}^{-1}$. The ‘best-fitting’ model of rotating disc describes primarily the latter motion, which seems to be related to the tidal flows seen in HI maps. However, the PA $\sim 70^\circ$, accounts for the former component. Thus, the H α kinematics gives additional evidence on the presence of a velocity component roughly in N–S direction, well seen in the high-resolution HI maps. The fainter HII region, 3 arcsec east of the main star-forming region, is situated along the direction, which is closer to the direction of the compact HI tidal protrusion, well seen in Fig. 5 of Ekta et al. (2009). By analogy with the discussed opportunity of stimulated SF in asymmetric shells prompted by tidal outflows in the case of E galaxy (Ekta et al. 2009), the similar situation can take place for W galaxy (albeit, with smaller power).

4.3.2 SBS 0335–052E

The ionized gas kinematics of SBS 0335–052E were studied by Izotov et al. (2006) on the limited region of 11×7 arcsec around the central star-forming regions. In that work the general velocity field was not discussed. Instead, they find the two-component H α -line profiles in several periphery regions, with component separation of $\sim 50 \text{ km s}^{-1}$, which were treated as the appearance of fast shells. In our obser-

vations we constructed the H α velocity field in the region of $\sim 17 \times 17$ arcsec in size.

Similar to the W component, we compare the motions of ionized gas in the E galaxy with that of HI gas in the same region. This comparison is conducted on the GMRT HI maps with the angular resolutions of ~ 20 arcsec and 9 arcsec. Since the respective analysis was already performed in Ekta et al. (2009), this allows us to look at the observed H α velocities in a more general context. Namely, there are two systems in the HI velocity field, which are identified with gas motions in elongated tidal tails. A longer and more rarefied one is directed in approximately SW-NE direction with velocities growing to the NE edge, that is in direction opposite to the position of the companion. A shorter, curved denser tail starts roughly in direction to NW and then bends to the W companion. For this tail (protrusion), the velocity decreases while gas travels further from the E galaxy. This direction is close to that of the asymmetric arc of ionized gas well seen in the *HST* V-band image of Thuan, Izotov & Lipovetsky (1997).

The coarse comparison of the observed H α velocity field in Fig. 2 with that of the described HI one, shows qualitative agreement. The region of minimal line-of-sight velocities at $\sim 6-7$ arcsec NW from the central starburst is close to the position of the arc. Thus, the effect of the expanding shell (visible as relative negative velocities on its front side) can also contribute to the structure of the velocity field. The significant swing of the isovelocity contours in the central region ($r \leq 10$ arcsec from the centre) seems may be related to the appearance of an expanding shell. To check how the disturbed velocity field looks like in the presence of a shell (in the zeroth approximation) we consider in the Appendix A several simulated velocity fields of rotating disc with a shell in different positions. The observed velocity field of SBS 0335-052E resembles that in our Model 3, which implies an off-centre location of the shell centre on the disc minor axis. Based on conclusions, obtained in Appendix A, we fixed the position angle of the model disc ($PA = 53^\circ$) in accord with the orientation of the large-scale HI structure. This model of rotation takes into account the main component of the velocity gradient (roughly from SW to NE). In the residual map one can clearly separate the same velocity minimum of the irregular form NW from the centre, related to the arc. The latter is natural to attribute to the approaching part of a shell, produced during a relatively recent episode of SF. Having in mind its irregular form, one can think of a superposition of two spatially close shells. Furthermore, the negative gradient in the NW direction is still visible, consistent with the similar flow seen along the HI NW tail.

It is worth noting the unusual behaviour in the model fit of rotation velocity in the very centre of the galaxy, at $r < 2$ arcsec. This can be treated as an appearance of kinematically decoupled counter-rotation, which could be a trace of merging gaseous clouds with the specific orientations of their angular momenta. However, the observed rotation velocities are too small. Therefore, the more probable option is that this a feature of the velocity field appears due to non-circular motions produced by a shell formed near the disc centre.

The galaxy SBS 0335-052E, unlike SBS 0335-052W, shows much more active star formation during the last sev-

eral hundred Myr. This induces both large-scale shells/arcs and increases the amplitude of chaotic (turbulent) motions. The local peculiarities of H α kinematics are better acquired by high-resolution spectra with VLT in Izotov et al. (2006). In particular, they detected wide-spread regions outside the central brightest clusters 1 and 2, where the line profiles are split on two components with velocity differences of ~ 50 km s $^{-1}$. The ‘broad’ lines with FWHM up to ~ 100 km s $^{-1}$ are present in these regions as well. While our angular resolution is about a factor of 1.7 worse, we also see in the corresponding regions the enhanced velocity dispersion of $\sim 60-70$ km s $^{-1}$, corresponding to FWHM ~ 150 km s $^{-1}$. Accounting for smoothing due to the worse seeing, these values look consistent. In fact, as the illustration in Fig. 1 shows, our data also hint at the two-peak structure of line profiles in the mentioned regions, but due to insufficient velocity resolution they can be treated only as an indication.

Summarising the overall ionized gas kinematics of the E galaxy, we conclude, that in accord with HI kinematics (Ekta et al. 2009), its direction of rotation is closer to the orbital plane. In general, we assume that before the merging galaxies experience coalescence, their innermost regions keep the information on their original rotation. In difference with the W galaxy case (polar collision), the collision of the E galaxy is closer to prograde or retrograde. As emphasized by Ekta et al. (2009), the latter may be one of the reasons of large differences in the current and earlier SFRs between E and W galaxies.

4.4 HS 0822+3542

The H α velocity field for this BCG is rather well fitted by the model of flat rotating disc. The rotation velocity curve raises up to ~ 13 km s $^{-1}$ at the radius $r = 3$ arcsec (~ 200 pc) and then falls to $\sim 7-9$ km s $^{-1}$ at radius of $r \sim 5-6$ arcsec. The region with the maximal residual velocity (of ~ 10 km s $^{-1}$) is positioned at a secondary peak of H α emission at $\sim 7-8$ arcsec NW of the main starburst region. This could be the brightest fragment of a large loop, a probable relic of a somewhat earlier star-forming episode. The comparison of H α kinematics with HI morphology and kinematics (see Chengalur et al. 2006) leads to interesting conclusions. At the highest angular resolution of ~ 6 arcsec, the related HI cloud is strongly elongated in the N-S direction. The brightest HII region is situated between two HI density peaks. Due to low S/N ratio, the HI velocity field is constructed only for the low-resolution datacube (beam ~ 25 arcsec). This has a general (but small) gradient in approximately N-S direction. However, in the vicinity of the optical body one can see the swing of isovelocity line, roughly in the direction close to the PA of H α velocity gradient.

The most probable reason for the formation of decoupled kinematic patterns - the internal as visible in ionized gas, and near polar orbits as outlined by HI - is the interaction with a nearby LSB dwarf SAO 0822+3545. The latter is also mapped in H α in the same observations and is discussed in a Subsection 4.9. This LSBD is situated at the projected distance of 3.8 arcmin (~ 15 kpc) and has line-of-sight velocity of only ~ 15 km s $^{-1}$ larger. It is ~ 3 times more massive in HI and ~ 0.35 mag more luminous in *B*-band than HS 0822+3542 (Pustilnik et al. 2003a; Chengalur et al.

2006). Therefore, one expects that the past interaction of the BCG progenitor with this LSBD could induce a starburst in HS 0822+3542.

Corbin et al. (2005), from their Hubble Space Telescope imaging of HS 0822+3542 with the spatial resolution of ~ 5 pc, found that its central SF region consists of two distinct components with projected separation of ~ 80 pc. Based on this morphology, they suggest that this very compact dwarf galaxy is currently being assembled from two tiny unrelated components. Our H α kinematics of this BCG, in difference to several other galaxies in this study, is rather well fit by a single disc [albeit disturbed by the earlier starburst(s) and related shell(s)]. This is difficult to match with the idea that the BCG is currently forming from two unrelated fragments.

It is worth noting that this H α kinematics and HI data from Chengalur et al. (2006) for HS 0822+3542 do not provide a comprehensive picture of the overall gas motions. Indeed, on one hand, the regular H α rotation within the whole region of optical emission (with the total extent of ~ 16 arcsec, or ~ 1 kpc), has an amplitude of ~ 13 km s $^{-1}$. On the other hand, HI data shows rotation with an amplitude of less than 5 km s $^{-1}$. At the moment it is unclear how much the beam-smearing affects the HI velocity data.

4.5 SDSS J1044+0353

In the SDSS colour image, this galaxy is elongated along the E–W direction, with an extent of ~ 10 arcsec. The extent along the N–S direction is ~ 4 arcsec. The brightest part, the ‘comet head’ on the W edge, is very blue; while the more diffuse tail with a second, eastern ‘peak’ at ~ 4 arcsec is somewhat redder. The analysis of surface brightness and colour radial dependencies by Papaderos et al. (2008) confirms this impression. They use the blue colours of a lower SB part of this object to infer the small ages of the underlying LSB disc. However, reservation are made on the possible significant contribution of nebular emission to its colour, that should be accounted for. Indeed, from our rather deep H α image, the extent of the galaxy nebular emission ($\sim 12 \times 8$ arcsec) appears to be similar to that of the SDSS continuum images.

The two-nuclei morphology of this galaxy is similar to that of other studied objects (HS 2236+1344, SBS 1159+545), for which their H α kinematics show good evidence for a merger event. The simple disc model that best fits the observed H α velocity field has the following parameters: $V_{\text{sys}} = 3865 \pm 1$ km s $^{-1}$, $PA = 273^\circ$, $i = 51^\circ$. The bright rotating core is well fit by a rotation centre shifted to the east by ~ 0.5 arcsec from the photometric centre. The maximal observed (not corrected for inclination) rotation velocity is 8–9 km s $^{-1}$. This peak is well seen on the model rotation curve in Fig. 5 at $r \sim 2$ arcsec. The residual velocities in the ‘core’ region ($r < 2.5$ arcsec) are small (< 5 km s $^{-1}$). In outer regions the regular rotation falls significantly, and the residual velocities amount up to 10–15 km s $^{-1}$. The fitting by a flat disc model with the maximal rotation velocity of ~ 10 km s $^{-1}$ results in rather small overall residuals. However, the two outer regions of the E component show residuals of up to ± 20 km s $^{-1}$. Namely in these regions we see a maximal velocity dispersion of up to 50 km s $^{-1}$. Besides, the radial dependence of rotation velocity is quite atypical

with a substantial fall after the maximum at $r \sim 2$ arcsec. This suggests that the gas kinematics of the eastern half of the galaxy are significantly disturbed. On the colour SDSS image, one can also see a redder, diffuse extension south of the main elongated body. All these properties are evidence for an unrelaxed state of this galaxy.

The available data are not sufficient to make a confident conclusion on the nature of this object. At the current level of understanding of its morphology and gas kinematics, the data do not contradict an idea that this is the result of a relatively minor, almost completed merger. Other interpretations look more problematical. The eastern component has a significantly smaller mass than the western one, in difference with, e.g., the case of HS 2236+1344. This results in a relatively weak velocity disturbance in the W component and a much fainter luminosity of E component in respect of that for W one. High-resolution HI mapping could probably produce a more complete picture of its dynamics during the last few hundred Myr.

4.6 SBS 1116+517 = Arp’s galaxy

This XMD BCG has a complex morphology in the central part, which consists of three knots with very different fluxes situated in a region with a total extent of ~ 5 arcsec (as first noticed by Arp 1965). The outer parts also show rather irregular morphology with finger-like protrusions, in particular on the S and E edges. While the full range of line-of-sight velocities in H α is more than 80 km s $^{-1}$, the velocity field is rather complex. It is hard to see tracers of regular rotation. Nevertheless, we try to construct the model of rotating disc for radial distances $r < 9$ arcsec, which we extrapolate to the outer region. The centre of the inner isophotes was set as the centre of rotation. As one expects, the rotation is indeed small: its maximal observed line-of-sight velocities are of order 5–10 km s $^{-1}$, while the residual velocities are ~ 20 km s $^{-1}$ in the central part and reach the value of ~ 50 km s $^{-1}$ at the E and SE periphery. The region with the most peculiar (redshifted) velocities is situated South-East from the bright ‘central’ knot and possibly represents the result of a merger (or infall to the disc).

While the ‘best-fitting’ model with rotation can account for maximal rotation velocity of ~ 10 – 12 km s $^{-1}$, the resulting residual velocity field shows the regions with values down to -20 km s $^{-1}$ and up to $+50$ km s $^{-1}$. This very disturbed velocity field, especially in outer parts of an ionized gas body, suggests strong perturbation. The presence of expanding shells from recent starbursts is probably one of the possible reasons. If one assigns the regions with the most negative velocities on the residual map to approaching fronts of such shells, their expansion velocities are ~ 20 km s $^{-1}$ and the total sizes are ~ 3 – 5 arcsec (or ~ 300 – 500 pc at the adopted distance of 23 Mpc). The sizes are quite typical of ionized-gas shells, visible in similar galaxies. However, the large positive residual velocity at the eastern edge of the galaxy is difficult to reconcile with shells. The morphology of H α -emission region and velocity fields, both the observed and residual, suggests strong external disturbance. No candidate galaxy capable of producing that strong of a disturbance is visible in the BCG environment. Therefore, the most natural interpretation that emerges from the study of SBS 1116+517 morphology and gas kinematics is the recent major merger

of dwarf galaxies, since for a minor merger one expects a relatively weak effect on the overall velocity field of the more massive component. If this picture is correct, one should expect that the HI morphology and velocity field are highly disturbed. Thus, this galaxy requires follow-up HI mapping with angular resolution of 3–5 arcsec.

4.7 SBS 1159+545

On the SDSS image SBS 1159+545 consists of two very blue knots (separated by ~ 5 arcsec, or ~ 1.3 kpc at the adopted distance of 52.5 Mpc), elongated roughly along NE–SW direction, with the luminosity difference of a factor ~ 2 . There are also redder lower brightness fragments; one is situated between the two blue knots and the other, with the total extent of ~ 5 arcsec, stretches as a tail of the fainter, blue SW knot. The SW knot itself has an extended structure, roughly oriented along E–W, and its redder tail looks like a continuation of this blue knot. On the other hand, the brighter NE knot also looks elongated on our narrow red continuum image, in a direction of S–N. This overall complex, curved morphology indicates a non-equilibrium state of this object.

The full range of H α velocities seen in our data is ~ 40 km s $^{-1}$. The velocity field is complex, and does not resemble a projected rotation. Moreover, it resembles that of some other objects in this study, with ‘two-nuclei’ morphology, which we have argued are mergers close to the full coalescence (SDSS J1044+0353 and HS 2236+1344). Namely, there are two local maxima in the line-of-sight velocity, close to the positions of the H α -emission peaks and a clear minimum along the border, or ‘middle’ lane, between these SF knots. From the position of this middle lane, the observed velocities grow to both NE and SW directions. However, after reaching the local maxima near the H α emission peaks they again fall. The largest velocities are seen on the W and E edges of the NE knot as well as at similar outer parts of the SW knot.

The velocity field model was built for the range $r < 5$ arcsec (with the centre at the NE knot) and was extrapolated to the SW knot. The ‘best-fitting’ model for the flat rotating disc centred on the brighter NE knot can account for only an amplitude of ~ 8 km s $^{-1}$ along the line-of-sight. The residual velocities are significantly larger, amounting on the knot’s east edge of 15–20 km s $^{-1}$. Similar indications of an overdisturbed velocity field come from the map of velocity dispersion. While in the regions around bright knots, this parameter does not exceed 15–20 km s $^{-1}$. In the E part of NE knot and the W part of the SW knot, this exceeds 30–50 km s $^{-1}$. The $PA = -13^\circ$ of the ‘best-fitting’ kinematic model significantly differs from $PA \approx 30^\circ$ of the apparent ‘disc’ plane – if the two knots were HII regions in the same disc galaxy. But this is consistent with the orientation of the NE knot itself, as seen from our narrow band continuum image. An attempt to interpret the whole velocity field as a result of combination of two expanding shells does not work. In this model, it is difficult to understand how the gas in the middle lane acquired its low observed velocity, while the line-of-sight velocities in the directions of expected centres of shells (NE and SW knots) show local maxima. Summarising this velocity field analysis, we suggest that from both the BCG morphology and gas velocity field,

the most plausible interpretation of the data is the merger of two dwarf galaxies.

4.8 HS 2236+1344

This XMD BCG also has the two-nuclei morphology with disturbed outer parts (Fig. 4). The separation of two bright knots, oriented in the N–S direction, is ~ 3 arcsec (or ~ 1.2 kpc in projection at the adopted distance of 85 Mpc). As seen in deep images (not shown here), the latter includes small tails protruding from both the northern edge of the N component (to the W) and from the southern part of the S component (Pustilnik et al., in preparation). These features already hint on the tidal perturbations in both components. Pramskij et al. (2003) studied the H α velocity field of this object with a long slit, positioned along the N–S direction. They discovered in the position-velocity diagram that the line-of-sight velocity makes a jump in the middle between the two knots. Our H α velocity field confirms that finding and adds important new features, including high velocity dispersion and large residual velocities near the regions of current starbursts for any model of single rotating disc.

The total velocity range is ~ 45 km s $^{-1}$. We attempted to fit the whole observed velocity field with the model of single flat rotating disc. Two variants of the circular motion model were constructed: (i) rotation centre coincides with the brighter (Southern) knot; (ii) rotation centre is fixed in the middle between Northern and Southern knots. However, both variants fail to reproduce the observed velocity gradients. For an alternative approach, the approximation of the overall H α velocity field by two rotating discs, positioned near the centres of S and N knots, gives a good fit with maximal rotation velocities of ~ 25 km s $^{-1}$ in both components (see Table 3 and Fig. 4 and 5). These discs have close PA , V_{sys} , i and maximal V_{rot} .

Due to lack of space, we focus on the model with two discs which provides a better fit to the observations than either single disc model. The map of velocity dispersion shows this parameter to be rather large in this BCG. Even its minimal values, located in the regions of both bright knots, are of ~ 25 km s $^{-1}$. In the adjacent regions, this parameter raises till 35–40 km s $^{-1}$, while in the outer parts, the velocity dispersion exceeds 50 km s $^{-1}$. The observed kinematics can not be explained as well by giant ionized shells in a single rotating disc. The latter are commonly expected to show negative relative velocities in their front edges, that is near the centres of star-forming regions, while the observed residuals are positive.

Taking into account all available morphological and kinematics data on this BCG, we conclude that the most likely nature of this object is a close strongly interacting pair of dwarf galaxies with comparable masses. It is quite probable that this pair is in the stage of merger close to full coalescence. This also provides a natural interpretation of the starbursts in both components. Indeed, as summarised by Begum et al. (2008), the late-type quiet dwarfs with that low V_{rot} have typical M_B in the range of -12.5 to -14.9 . Therefore, the $M_B = -16.9$ for HS 2236+1344 indicates a very strong starburst.

4.9 Properties of two by-product LSB galaxies

In this section we briefly discuss two galaxies that appeared sufficiently close on spatial and velocity separation to the main studied XMD galaxy and were mapped along with the main target.

4.9.1 Anon J012544+075957

In the FPI datacube for UGC 993, an LSB dwarf galaxy Anon J012544+075957 appeared (see bottom of Table 2) at 2.5 arcmin East and ~ 40 arcsec North from the main target (~ 29 kpc in projection). Its line-of-sight velocity (as found here from its $H\alpha$ velocity field) is ~ 70 km s $^{-1}$ larger than the mean velocity of the UGC 993 system. Its $H\alpha$ image (Fig. 4) displays three main regions elongated roughly from NE to SW, forming the main body with the total extent of ~ 25 arcsec and a separate faint knot SW from this. The velocity range along the body is ~ 70 km s $^{-1}$. The ‘best-fitting’ model parameters for a rotating thin disc are as follows: $V_{\text{sys}}=3012$ km s $^{-1}$, $PA=324^\circ$, $i=64^\circ$. The resulting rotation curve reaches a maximum value of ~ 25 km s $^{-1}$ (Fig. 5) at the edge of the $H\alpha$ map ($r \sim 12$ arcsec). The gas morphology of this LSB galaxy is clearly disturbed and elongated nearly perpendicular to the plane of rotation. It is interesting that in the blue continuum, the galaxy looks less elongated than in $H\alpha$. However, there are two extensions approximately to the N and S, close to the elongation of $H\alpha$ emission. The velocity dispersion near the peaks of $H\alpha$ emission is a modest ~ 25 km s $^{-1}$. In some of the outer regions, it raises up to 60-70 km s $^{-1}$, but this is probably attributed to a low S/N ratio.

Along with the already discussed two kinematically decoupled components of UGC 993, this dwarf Irr galaxy likely comprises a progenitor triplet of low-mass galaxies, whose common dynamical evolution resulted in a recent merger, as seen in UGC 993. The general problem of such dwarf bound systems was addressed, in particular, in Tully et al. (2006).

4.9.2 SAO 0822+3545

Another by-product object, SAO 0822+3545, the LSB dwarf galaxy, known as a companion of HS 0822+3542, was already discussed in Pustilnik et al. (2003a). Its unusually blue BVR colours imply a rather small age for its main stellar population. Low level SF in this LSBD was noted in the latter study based on the detection of a low EW $H\alpha$ emission in the long-slit spectrum taken along the major axis. The new data show the 2D distribution of $H\alpha$ emission (see Fig. 4) and allow us to perform a more careful analysis of SF issues.

In particular, our $H\alpha$ image shows that the current SF in this LSB dwarf is highly inhomogeneous. It is concentrated in two close HII regions No. 1 and 2 (~ 4 arcsec, or ~ 0.26 kpc in between) at the Northern edge of the main galaxy body, where no light concentration is seen in the broad-band continuum images. A fainter $H\alpha$ protrusion is seen in the W part of the faint irregular structure. The $H\alpha$ kinematics are complex. On one hand, due to very limited spatial coverage of $H\alpha$ emission over the LSBD body, it is difficult to derive the parameters of a rotating disc model

based only on $H\alpha$ data. On the other hand, the $H\alpha$ velocities are in good agreement in the overlapping regions with those observed in HI as presented in Chengalur et al. (2006). Based on this fact, we fixed the position of the rotation centre, PA , and i , as they emerge from the mentioned HI maps.

As usual, the velocity dispersion near the brightest $H\alpha$ knots is rather low: ~ 5 -15 km s $^{-1}$. In several regions outside these two knots, where $H\alpha$ is still seen - at ~ 4 arcsec SE of knot No. 1 and in the W protrusion - the velocity dispersion is large, up to 60-70 km s $^{-1}$. This could be evidence of recent strong disturbances of the galaxy’s ISM. We also notice that the total $H\alpha$ flux in this LSB galaxy is ~ 25 times smaller than that in its companion BCG HS 0822+3542, while its total blue luminosity is ~ 30 per cent higher (Pustilnik et al. 2003a). This seemingly reflects the difference between the SF properties in the two interacting galaxies, related to the difference in their density distribution and the strength of the tidal trigger.

5 SUMMARY

Summarising the results and discussion above, we draw the following conclusions:

(i) The ionized gas kinematics in very low-metallicity star-forming galaxies, studied with FPI $H\alpha$ observations are significantly disturbed and rarely can be well fitted by only single disc with regular rotation.

(ii) Several of our galaxies show more or less clear evidence from morphology and $H\alpha$ velocity fields for various stages of mergers (UGC 993, SDSS J1044+0353, SBS 1116+517, SBS 1159+545, HS 2236+1344). In two cases we have good evidence for two independently rotating discs (UGC 993 and HS 2236+1344).

(iii) In the other galaxies, the rotation component of the overall velocity field is important, but large disturbances appear. The residuals of the ‘best-fitting’ rotation model imply either a recent merger, or sufficiently strong disturbance by nearby galaxies (HS 0822+3542 and UGC 772).

(iv) Probable starburst-induced shells were identified in several galaxies (UGC 772, UGC 993, SBS 0335-052E, SBS 1116+517) through their ionized gas velocity fields and velocity dispersion maps. We presented the results of simple simulations of the expected velocity patterns which one can observe in dwarf galaxies with expanding shells. To first order, this allowed a feel for the effect of shells on the results of the tilted-ring model.

(v) The interacting/merging nature of the binary system of the well separated XMD galaxies SBS 0335-052E and W is best evident from their HI morphology and kinematics data. Despite a relatively large mutual distance, the tidal action of each component to the other clearly affects the gas dynamics of these very gas-rich objects and triggers the current SF burst and very likely the previous major SF episode (as emphasized by Ekta et al. 2009). To understand this unique interacting system (a nice representative of high-redshift young galaxies) in more detail, one needs a wide grid of models of interacting gas-rich galaxies, like, e.g., “Identikit” (Barnes & Hibbard 2009), but including SF processes.

(vi) The $H\alpha$ images and velocity fields for two LSB

dwarfs, Anon J012544+075957 and SAO 0822+3545, companions of two program XMD galaxies, are obtained and analysed. They can be used in statistical studies of SF in LSB dwarfs. The star formation in SAO 0822+3545 is highly asymmetric and takes place mainly in two knots at the northern edge, that is likely induced by the recent interaction with the nearby XMD BCG HS 0822+3542.

The statistics of XMD starbursting galaxies, for which kinematics of gas were studied in detail, is still insufficient. Nevertheless, the results of our FPI study of the ionized gas kinematics in the subsample of nine XMD star-forming galaxies, along with the complementary results of the GMRT HI study of a part of these and other XMD galaxies (Ekta et al. 2008, 2009; Ekta & Chengalur 2010), indicate that strong interactions and mergers of very metal-poor dwarf galaxies are one of the major or significant factors triggering their current and recent starbursts. In particular, this is valid for the six most metal-poor ($12+\log(\text{O}/\text{H}) < 7.30$) dwarf starbursting galaxies. Merger-induced starbursts are consistent with the idea that the progenitors of such rare objects either are old and have been evolving very slowly on the cosmological timescale before the current starburst have occurred, or they are extremely metal-poor because they are comparatively young, and thus began their star formation and chemical enrichment with large delay.

ACKNOWLEDGEMENTS

This research has made use of the NASA/IPAC Extragalactic Database (NED) which is operated by the Jet Propulsion Laboratory, California Institute of Technology, under contract with the National Aeronautics and Space Administration. Funding for the Sloan Digital Sky Survey (SDSS) and SDSS-II has been provided by the Alfred P. Sloan Foundation, the Participating Institutions, the National Science Foundation, the US Department of Energy, the National Aeronautics and Space Administration, the Japanese Monbukagakusho, the Max Planck Society and the Higher Education Funding Council for England. The SDSS web site is <http://www.sdss.org/>. AVM and SAP acknowledge the support of this work through RFBR grant No. 06-02-16617. AVM also acknowledges the support from RFBR grant No. 09-02-00870. AYK and SAP acknowledge support from the National Research Foundation of South Africa. We thank B. Ekta and J. Chengalur for providing us with new information on HI morphology and velocity field of some of the studied XMD galaxies prior publication, and A. Burenkov for the help with observations. We are grateful to S. Crawford for the help in English improvement. The authors thank the anonymous referee for useful suggestions and questions, which helped to improve the paper.

REFERENCES

- Afanasiev, V.L., Moiseev A.V., 2005, *Astron. Lett.*, 31, 193
 Arp H., 1965, *ApJ*, 142, 402
 Asplund, M., Grevesse, N., Sauval, A. J., Allende Prieto, C., Kiselman, D., 2004, *A&A*, 417, 751
 Barnes J.E., Hibbard J.E., 2009, *AJ*, 137, 3071
 Begum A., Chengalur J.N., Karachentsev I.D., Kaisin S.S., Sharina M.E., 2006, *MNRAS*, 365, 1220
 Begum A., Chengalur J.N., Karachentsev I.D., Sharina M.E., Kaisin S.S., 2008, *MNRAS*, 386, 1667
 Bekki K., 2008, *MNRAS*, 388, L10
 Bordalo V., Plana H., Telles E., 2009, *ApJ*, 696, 1668
 Brosch N., Almoznino E., Heller A.B., 2004, *MNRAS*, 349, 357
 Brown W.R., Kewley L.J., Geller M.J., 2008, *AJ*, 135, 92
 Chengalur J.N., Pustilnik S.A., Martin J.-M., Kniazev A.Y., 2006, *MNRAS*, 371, 1849
 Conselice C.J., 2003, *ApJS*, 147, 1
 Conselice C.J., 2006, *MNRAS*, 373, 1389
 Corbin M.R., Vacca W.D., Hibbard J.E., Somerville R.S., Windhorst R.A., 2005, *ApJ*, 629, L89
 Di Matteo P., Bournaud F., Martig M., Combes F., Melchior A.-L., Semelin B., 2008, *A&A*, 492, 31
 Ekta B., Chengalur J.N., 2010, *MNRAS*, 2010MNRAS.tmp...69E
 Ekta, Chengalur J.N., Pustilnik S.A., 2006, *MNRAS*, 372, 853
 Ekta, Chengalur J.N., Pustilnik S.A., 2008, *MNRAS*, 381, 881
 Ekta B., Pustilnik S.A., Chengalur J.N., 2009, *MNRAS*, 397, 963
 García-Lorenzo B., Cairós L.M., Caon N., Monreal-Ibero A., Kehrig C., 2008, *ApJ*, 677, 201
 Guseva N.G., Papaderos P., Meyer H.T., Izotov Y.I., Fricke K.J., 2009, *A&A*, 505, 63
 Icke V., 1985, *A&A*, 144, 115
 Izotov Y.I., Thuan T.X., 2007, *ApJ*, 665, 1115
 Izotov Y.I., Thuan T.X., Guseva N.G., 2005, *ApJ*, 632, 210
 Izotov Y.I., Schaerer D., Blecha A., Royer F., Guseva, N.G., North P., 2006, *A&A*, 459, 71
 Izotov Y.I., Guseva N.G., Fricke K.J., Papaderos P., 2009, *A&A*, 503, 61
 Jesseit R., Naab T., Peletier R., Burkert A., 2007, *MNRAS*, 376, 997
 Kakazu Y., Cowie L.L., Hu E.M., 2007, *ApJ*, 668, 853
 Kniazev A.Y., Grebel E.K., Hao L., Strauss M., Brinkmann J., Fukujita M., 2003, *ApJ*, 593, L73
 Kronberger T., Kapferer W., Schindler S., Böhm A., Kutdemir E., Ziegler, B.L., 2006, *A&A*, 458, 69
 Kunth D., Östlin G. 2000, *A&ARv*, 10, 1
 Lee J.C., Kennicutt R.C., Funes J., Sakai S., Akiyama S., 2009, *ApJ*, 692, 1305
 Lotz J.M., Jonsson P., Cox T.J., Primack J.R., 2008, *MNRAS*, 391, 1137
 Lozinskaya T.A., Moiseev A.V., Avdeev V.Y., Egorov O.V., 2006, *Astron. Lett.*, 32, 361
 Martin C.L., 1996, *ApJ*, 465, 680
 Martin C.L., 1998, *ApJ*, 506, 222
 Martínez-Delgado I., Tenorio-Tagle G., Muñoz-Tunión C., Moiseev A.V., Cairós L.M., 2007, *AJ*, 133, 2892
 Melbourne J., Salzer J.J., 2002, *AJ*, 123, 2302
 Moiseev A.V., 2002, *Bull. Spec. Astrophys. Obs.* 54, 74 (arXiv:astro-ph/0211104)
 Moiseev A.V. 2008, *Astrophys. Bull.*, 63, 201 (arXiv:0808.1696/astro-ph)
 Moiseev A.V., Valdés J.R., Chavushyan V.H., 2004, *A&A*, 421, 433
 Moiseev A.V., Egorov O.V., 2008, *Astrophys. Bull.* 63, 193

- Moustakas J., Kennicutt Jr. R.C. 2006, *ApJS*, 164, 81
- Noeske K.G., Iglesias-Páramo J., Vilchez J.M., Papaderos P., Fricke K.J., 2001, *A&A*, 371, 806
- Östlin G., Amram P., Bergvall N., Masegosa J., Boulesteix J., 1999, *A&AS*, 147, 419
- Östlin G., Amram P., Bergvall N., Masegosa J., Boulesteix J., Márquez I., 2001, *A&A*, 374, 800
- Papaderos P., Guseva N.G., Izotov Y.I., Fricke K.J., 2008, *A&A*, 491, 113
- Pedrosa S., Tissera P.B., Fuentes-Carrera I., Mendes de Oliveira C., 2008, *A&A*, 484, 299,
- Pelupessy F.I., van der Werf P.P., Icke V., 2004, *A&A*, 422, 55
- Pérez-Gallego J., Guzmán R., Castillo-Morales A., et al. 2009, *MNRAS*, accepted (arXiv:0911.1069)
- Petrosian A., Comte G., Boulesteix J., Kunth D., Movsesian T., Dodonov S., Le Coarer E., Burenkov A., 1995, *Astrofizika*, 38, 335
- Pramskij A., Pustilnik S., Kniazev A., Ugryumov A., 2003, *SAO RAS preprint No. 189*.
- Puech M., Hammer F., Flores H., Östlin G., Marquart T., 2006, *A&A*, 455, 119
- Pustilnik S.A., Kniazev A.Y., Lipovetsky V.A., Ugryumov A.V., 2001a, *A&A*, 373, 24
- Pustilnik S.A., Brinks E., Thuan T.X., Lipovetsky V.A., Izotov Y.I., 2001b, *AJ*, 121, 1413
- Pustilnik S.A., Kniazev A.Y., Pramsky A.G., Ugryumov A.V., Masegosa J., 2003a, *A&A*, 409, 917
- Pustilnik S.A., Zasov A.V., Kniazev A.Y., Pramsky A.G., Ugryumov A.V., Burenkov A.N., 2003b, *A&A*, 400, 841
- Pustilnik S.A., Kniazev A.Y., Pramsky A.G., Ugryumov A.V., 2003c, *Ap.Spa.Sci.*, 284, 795
- Pustilnik S.A., Kniazev A.Y., Pramsky A.G., Izotov Y., Foltz C., Brosch N., Martin J.-M., Ugryumov A.V., 2004a, *A&A*, 419, 469
- Pustilnik S., Pramskij A., Kniazev A., 2004b, *A&A*, 425, 51
- Pustilnik S.A., Engels D., Lipovetsky V.A., et al. 2005a, *A&A*, 442, 109
- Pustilnik S.A., Kniazev A.Y., Pramskij A.G., 2005b, *A&A*, 443, 91
- Pustilnik S.A., Engels D., Kniazev A.Y., Pramskij A.G., Ugryumov A.V., Hagen H.-J., 2006, *Astron.Lett.* 32, 228
- Pustilnik S.A., Martin J.-M., 2007, *A&A*, 464, 859
- Pustilnik S.A., 2008, in: *Dark Galaxies and Lost Baryons*, Proc. of IAU Symposium No. 244, p. 341, eds. J. Davies and M. Disney, Cambridge University Press, Cambridge.
- Pustilnik S.A., Tepliakova A.L., Kniazev A.Y., 2008, *Astron.Lett.*, 31, 457 (arXiv:0712.4007)
- Pustilnik S.A., Tepliakova A.L., Kniazev A.Y., J.-M.Martin, Burenkov A.N., 2010, *MNRAS*, 401, 333
- Salzer J.J., Norton S.A., 1999, in Proc. of IAU colloquium "Low Surface Brightness Universe", ASP Conference Series 170, Eds. J.I. Davies, C. Impey, & S. Phillipps, p. 253
- Schlegel D.J., Finkbeiner D.P., Douglas M., 1998, *ApJ*, 500, 525
- Smoker J.V., Davies R.D., Axon D.J., 1996, *MNRAS*, 281, 393
- Staveley-Smith L., Davies R.D., Kinman T.D., 1992, *MNRAS*, 258, 334
- Taylor C.L., Brinks E., Grashuis R.M., Skillman E.D. 1995, *ApJS*, 99, 497
- Teuben P.J., 2002, in 'Disks of Galaxies: Kinematics, Dynamics and Perturbations', ASP Conference Proceedings 275, Eds. E. Athanassoula, A. Bosma, & R. Mujica, 217
- Thuan T.X., Izotov Y.I., Lipovetsky V.A., 1997, *ApJ*, 477, 661
- Tully R.B., Rizzi L., Dolphin A.E., Karachentsev I.D., Karachentseva V.E., Makarov D.I., Makarova L., Sakai S., Shaya E.J., 2006, *AJ*, 132, 729
- Tully R.B., Shaya E.J., Karachentsev I.D., Courtois H.M., Kocevski D.D., Rizzi L., Peel A., 2008, *ApJ*, 676, 184
- Ugryumov A.V., Engels D., Pustilnik S.A., Kniazev A.Y., Pramskij A.G., & Hagen H.-J., 2003, *A&A*, 397, 463
- Zasov A.V., Kniazev A.Y., Pustilnik S.A., Pramsky A.G., Burenkov A.N., Ugryumov A.V., Martin J.-M., 2000, *A&AS*, 144, 429
- van Zee L., Westpfahl D., Haynes M., Salzer J.J., 1998, *AJ*, 115, 1000
- Yang Y., Flores H., Hammer F., et al., 2008, *A&A*, 477, 789

APPENDIX A: ON THE VELOCITY FIELD OF DISC WITH SUPERIMPOSED SHELL

The tilted-ring fit is very popular for analysis of gas velocity fields in galactic discs (see Teuben (2002) for detailed review). In this approach, it is easy to connect the radial trends of kinematically determined PA and i with real changes of disc geometrical parameters (warp, polar rings, etc.) and/or with regular non-circular motions caused by spiral arms or bar. However, in dwarf galaxies the SF-induced expanding shells can significantly disturb the disc velocity field since the amplitude of the rotation curve is rather small and the size of a shell can be comparable with the size of the disc. If we allow for variations of kinematical PA with radius, it can lead to a mistaken conclusion on disc orientation or about the character of non-circular motions. In this Appendix we examine the effect of expanding shells on the tilted-ring fitting of artificial velocity fields.

The ‘observed’ velocities in our two-component model are simply the sum of line-of-sight velocities for the disc and the shell:

$$V_{obs} = V_{disc} + V_{shell} = V_{sys} + V_{rot} \cos \varphi \sin i + V_{shell}. \quad (A1)$$

This approximation assumes the equal contribution of both components in the total velocity pattern in the overlapping regions, i.e., the same brightness of the components in each point. Of course, this is not similar to the real situation. However, we believe that eq. (A1) can be used as a first approximation. One of the constraints used in the models below is that V_{shell} should not exceed the typical $FWHM$ of the observed emission lines (about $30 - 50 \text{ km s}^{-1}$). Otherwise we would detect the two-component line profiles.

The azimuthal angle in the plane of galaxy φ is connected with the position angle in the sky by the relation: $\tan \varphi = \tan(PA - PA_0) / \cos i$. The rising rotation curve is constructed by the relation:

$$V_{rot} = \frac{2}{\pi} V_{max} \arctan \frac{R}{h}, \quad (A2)$$

with $h = 1 \text{ arcsec}$ and the maximal velocity $V_{max} = 30 \text{ km s}^{-1}$ which is typical of dwarf galaxies in our sample.

For the shell, we use a model of a thin expanding hemisphere. This implies that we see only its approaching (blueshifted) side, whereas the redshifted one is obscured by an interior extinction. The model for the shell is:

$$V_{shell} = -V_{exp} \sqrt{1 + \frac{(x - x_s)^2 + (y - y_s)^2}{R_s^2}}. \quad (A3)$$

Here x_s and y_s are sky-plane coordinates of the shell centre relative to the disc centre. The shell has a radius of $R_s = 3.5 \text{ arcsec}$ and the expansion velocity of $V_{exp} = 15 \text{ km s}^{-1}$.

Using eq. (A1), we created models for moderately inclined disc ($i = 45^\circ$, $PA_0 = 45^\circ$) with the maximal radius of 10 arcsec and with various values of x_s and y_s . A systemic velocity of $V_{sys} = 1000 \text{ km s}^{-1}$ was adopted, that is representative of our sample. Its value has no effect on model isovelocity patterns.

The models were calculated on the grid with cell size 0.1 arcsec . Then the constructed models were convolved with the 2D Gaussian with $FWHM = 1.5 \text{ arcsec}$ that simulated the typical seeing effect, and were rebinned with the pixel

size of 0.5 arcsec in accord with our observational conditions. Fig. A1 shows examples of typical simulated velocity fields.

Model 0 represents the disc without shell. In Model 1 the shell is located in the disc centre. In Model 2 and Model 3, the centre of the shell is shifted along the major and the minor axes, respectively. In Model 4 the shell centre is shifted in the direction of $PA = 180^\circ$.

The simulated velocity fields were analysed with the same tilted-ring model method under two approximations. Method I allows for radial variations of PA and V_{sys} , while in Method II these values were fixed and only the rotation velocity was a free parameter. The inclination angle and the rotation centre were fixed in both Methods. Fig. A1 shows the residual velocities in the both approximations. The results of fitting are shown in Fig. A2. These figures demonstrate how an expanding shell affects the observed velocity field and changes the estimates of best-fitting parameters. Namely, the central location of the shell, or its offset along the disc major axis provoke the radial variations of V_{sys} (see Models 1 and 2). The shell location beyond the disc major axis also gives the systematic errors in the PA estimations (Models 3 and 4). When the shell centre lies on the minor axis, the radial trend of PA reach the maximal amplitude ($\sim 20^\circ$ in our simulations). That large variation of PA can result in erroneous conclusions concerning the disc structure, like the presence of the inner warp or even of a nuclear disc.

The residual velocities in the case of Method I seem spread over a larger portion of the disc than the real area of the shell (Fig. A1). The residuals are relatively small, usually about $\pm 5-7 \text{ km s}^{-1}$. Moreover, the peak of negative (‘blue’) residuals usually does not coincide with the centre of the shell. In contrast, if PA and V_{sys} are constant (i.e., for Method II), the residual velocities pattern is in a good agreement with the location of the shell, and the value of the negative residuals is consistent with V_{exp} , with except of the special case of Model 2.

It is worth noting that the rotation curve derived from the simulated velocity field can be distorted independently of the analysis method, as can be seen for V_{rot} plots for Models 2 and 4 in Fig. A2. However, in the Method II approach, we can unambiguously recognise from the residual map the perturbed portion of the disc and then derive the real rotation curve on the second iteration after masking the shell region. The latter is impossible if PA and V_{sys} are free parameters of the fitting, because in this case it is difficult to recognise the shell location.

Based on the results presented above, we have analysed the velocity fields of dwarf galaxies using the ‘tilted-ring’ fitting assuming that PA and V_{sys} are constant with radius. When the first approximation was done, we masked the regions with large residuals (usually, larger than $5-10 \text{ km s}^{-1}$) and repeated the fitting. The final model velocity field and the rotation curve, i.e., parameters of the disc orientation were calculated after several such iterations.

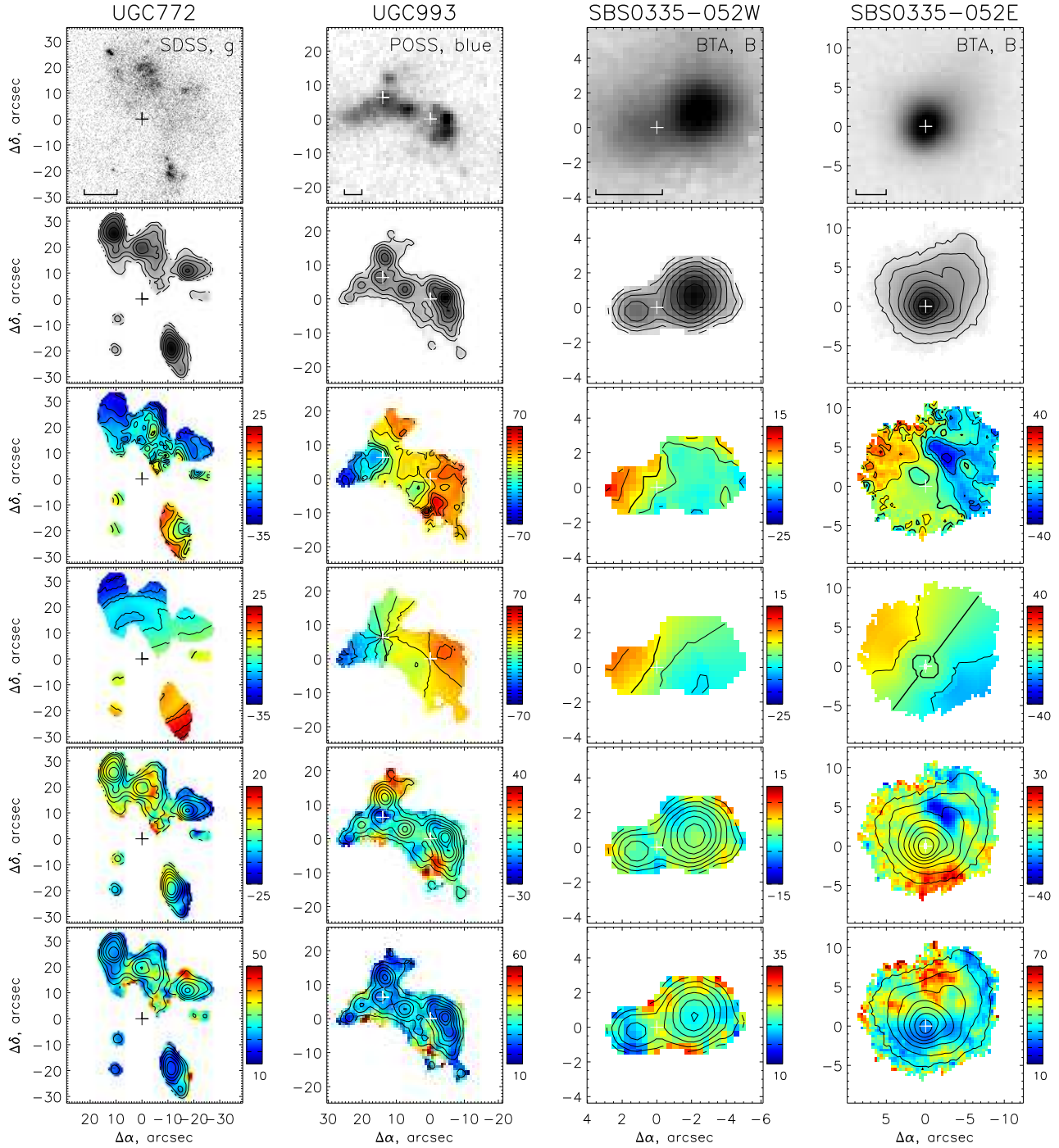


Figure 2. Images and FPI maps for four program galaxies UGC 772, UGC 993, SBS 0335–052W and SBS 0335–052E. From top to bottom: broad-band and $H\alpha$ images in logarithmic intensity scale; the line-of-sight velocity field in $H\alpha$ and model of circular-rotated disc, the scale is in km s^{-1} relative to the systemic velocity which is corresponded to thick contour; the maps of residual velocities and of velocity dispersion. In two latter maps the isophotes of $H\alpha$ -line intensity are also superimposed. The cross marks the kinematic centre. For UGC 993 and HS 2236+1344, centres of both discussed components are marked. The step between isoveLOCITIES is 5 km s^{-1} , with the exception of UGC 993, SBS 0335–052E and Anon J012544+075957 where the step of 10 km s^{-1} was used. The scale bar in the top panel corresponds to 1 kpc.

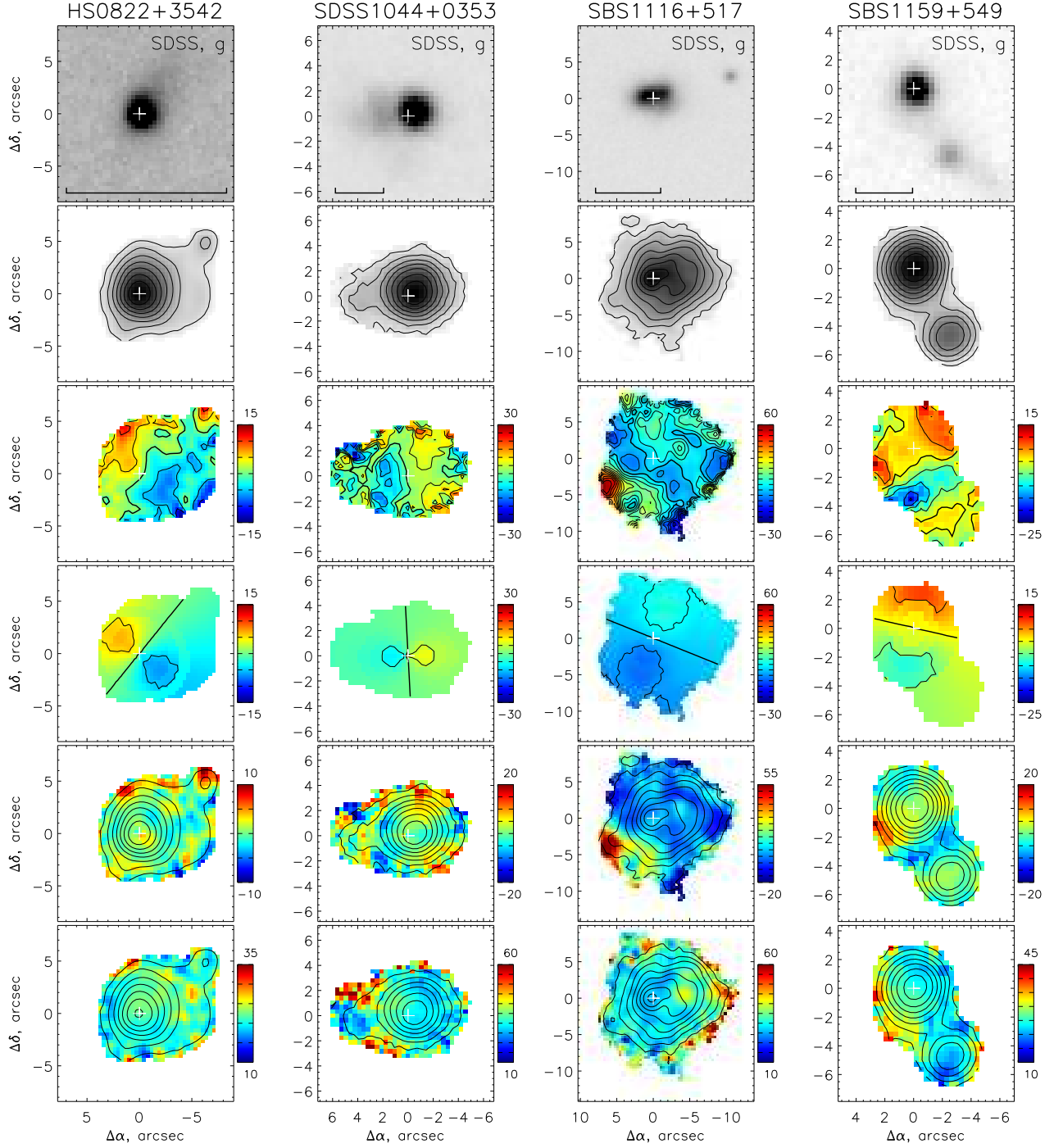


Figure 3. Same as in Fig. 2, but for galaxies HS 0822+3542, SDSS J1044+0353, SBS 1116+517 and SBS 1159+549.

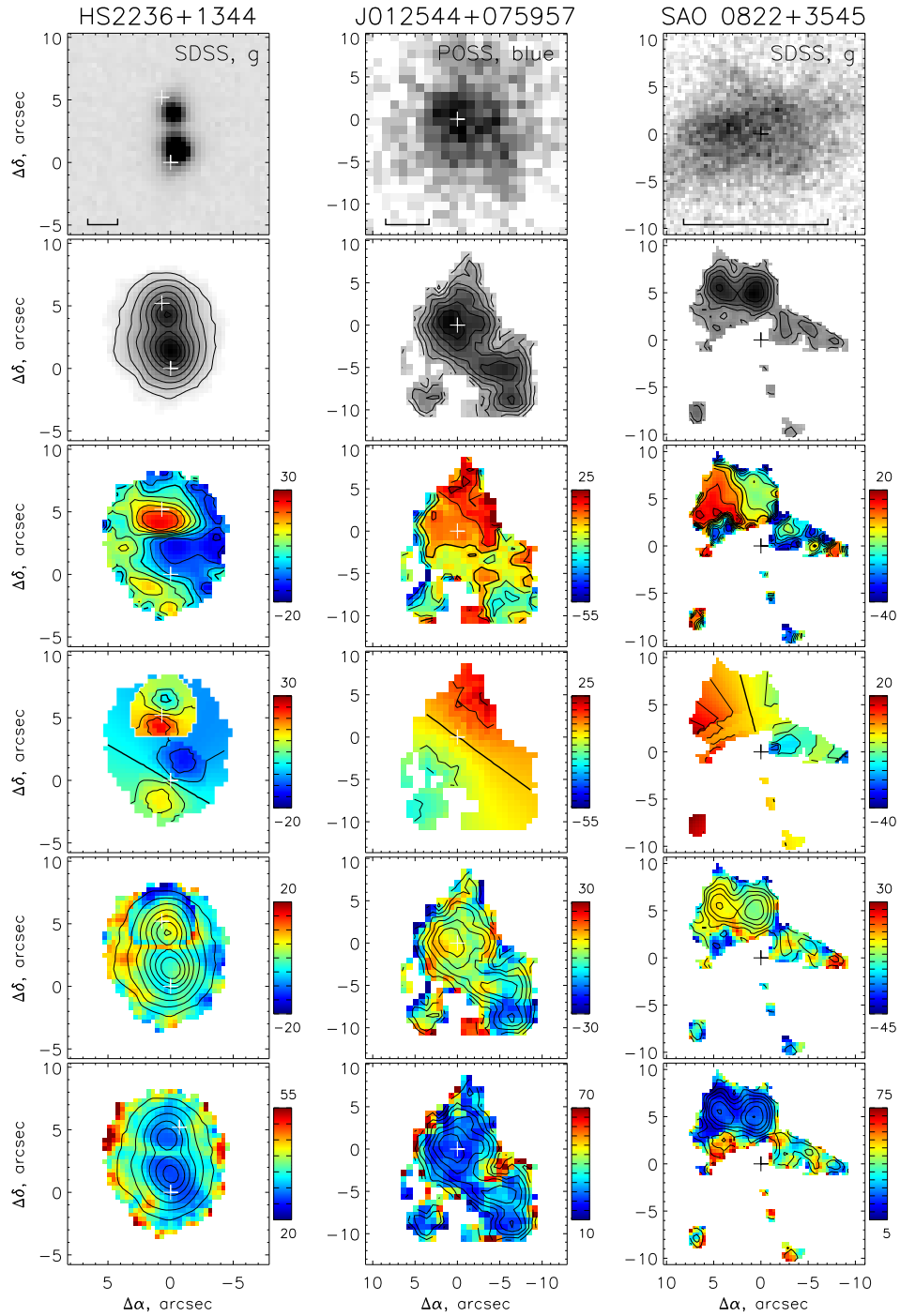


Figure 4. Same as in Fig. 2, but for XMD galaxy HS 2236+1344 and for two by-product LSB galaxies Anon J012544+075957 and SAO 0822+3545.

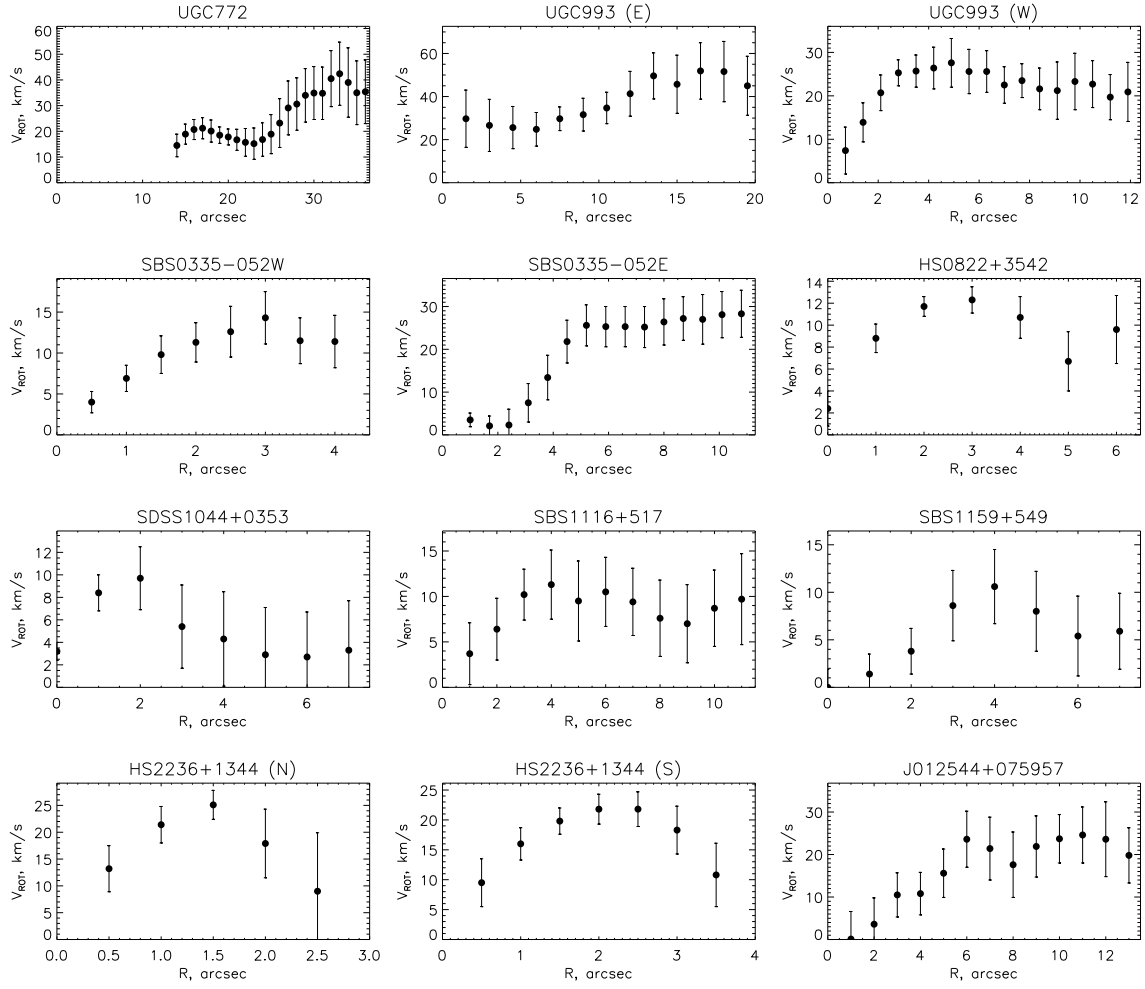


Figure 5. Radial dependence of rotation velocity in the best-fitting models for all discussed objects.

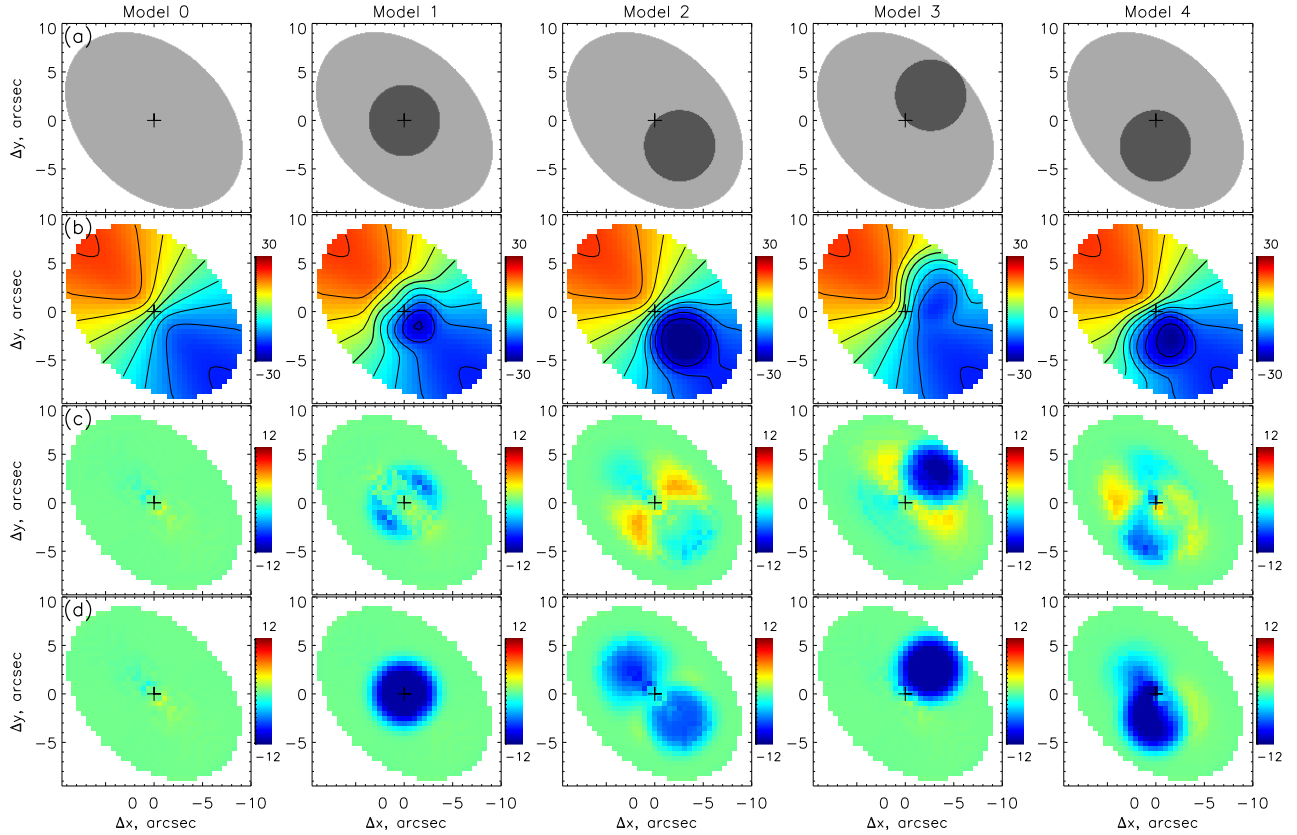


Figure A1. The simulated maps. (a) – the relative position of the disc (grey) and shell (dark). (b) – the simulated velocity field (after the subtraction of $V_{sys} = 1000 \text{ km s}^{-1}$). (c) – the residual velocity field after the subtraction of the tilted-ring model (Method I) which allows variations of PA and V_{sys} . (d) – the same residual field, but for Method II ($PA, V_{sys} = \text{const}$)

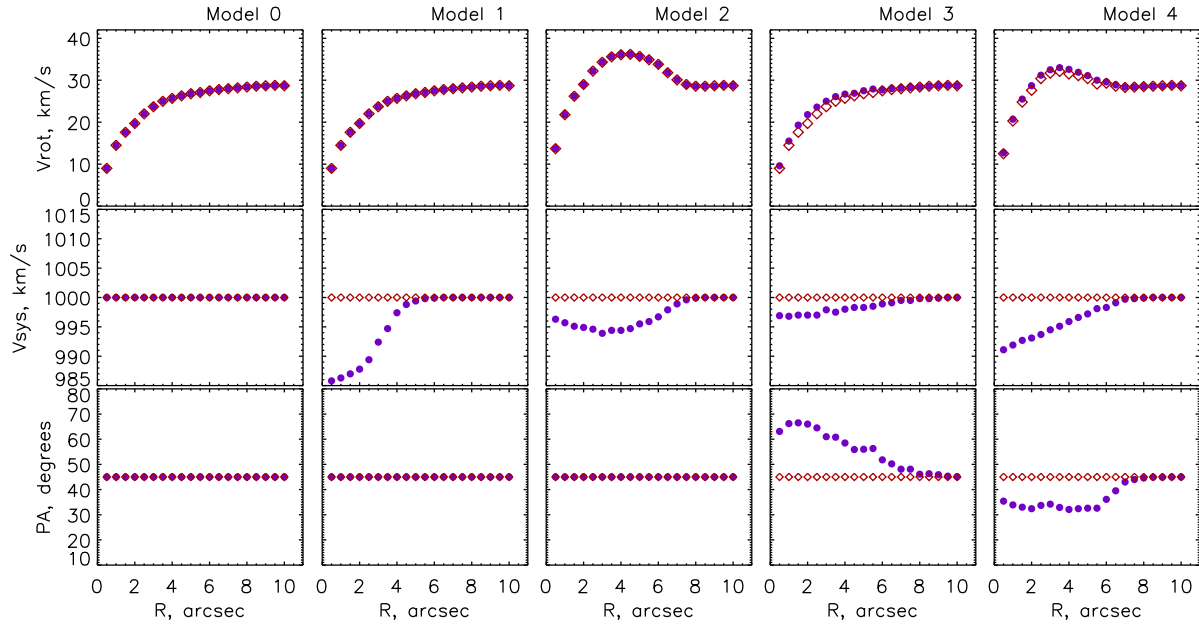


Figure A2. The fitting parameters for the simulated velocity fields: rotation velocity (top), position angle (middle) and systemic velocity (bottom). Blue points and red diamonds show results for Method I and Method II, respectively.